Supporting Information for

CO Reduction to CH_3OSiMe_3: Electrophile-Promoted Hydride Migration at a Single Fe Site

Meaghan M. Deegan and Jonas C. Peters

Division of Chemistry and Chemical Engineering
California Institute of Technology
Pasadena, CA 91125 United States

Table of Contents

1. Experimental Details

1.1 General Considerations

All manipulations were carried out using standard Schlenk or glovebox techniques under an N_2 atmosphere. Solvents were deoxygenated and dried by thoroughly sparging with N_2 followed by passage through an activated alumina column in a solvent purification system by SG Water, USA LLC. THF was dried further by stirring over Na/K (>2 h) and was filtered through Celite prior to use. Deuterated solvents were purchased from Cambridge Isotope Laboratories, Inc., degassed, and dried over activated 3 Å molecular sieves before use. Reagents were purchased from commercial vendors and used without further purification unless otherwise noted. $P_3^B(\mu\text{-H})Fe(H)(CO)$ **1** was prepared according to a literature procedure.[1] Labeled analogs of **1** (**1-D_2**, **1-^{13}CO**, and **1-D_2/^{13}CO**) were prepared analogously using ^{13}CO and D_2 gases.

1.2 Physical Methods

NMR spectra (^1H, ^{13}C, ^{31}P, ^{11}B, and ^{29}Si) were collected at room temperature (25 °C unless specified) on Varian 300, 400, or 500 MHz spectrometers. ^1H, ^{13}C, and ^{29}Si chemical shifts are reported in ppm, relative to tetramethylsilane using residual proton and ^{13}C resonances from solvent as internal standards. ^{31}P chemical shifts are reported in ppm relative to 85% aqueous H_3PO_4 and ^{11}B spectra were referenced to $BF_3 \bullet Et_2O$. Thin film IR spectra were obtained using a Bruker Alpha Platinum ATR spectrometer with OPUS software in a glovebox under an N_2 atmosphere. UV-vis measurements were collected using a Cary 50 instrument with Cary WinUV software. X-band EPR spectra were obtained on a Bruker EMX spectrometer on solutions prepared as frozen glasses in 2-MeTHF. Spectra were simulated using the EasySpin[2] suite of programs with MatLab. Mössbauer spectra were recorded on a spectrometer from SEE Co. (Edina, MN) operating in the constant acceleration mode in a transmission geometry. The sample was kept in an SVT-400 cryostat from Janis (Wilmington, MA). The quoted isomer shifts are relative to the centroid of the spectrum of a metallic foil of α-Fe at room temperature. Solution samples were prepared by freezing solutions in a Delrin cup in a glovebox with rapid transfer of frozen samples to a liquid nitrogen bath before mounting in the cryostat. Samples were collected with no applied magnetic field unless otherwise specified. Data analysis was performed using the program WMOSS (www.wmoss.org) and quadrupole doublets were fit to Lorentzian lineshapes.

X-Ray diffraction and combustion analysis measurements were carried out in the Beckman Institute Crystallography Facility. XRD measurements were collected using a dual source Bruker D8 Venture, four-circle diffractometer with a PHOTON CMOS detector. Structures were solved using SHELXT and refined against F^2 on all data by full-matrix least squares with SHELXL. The crystals were mounted on a glass fiber under Paratone N oil. See below for any special refinement details for individual data sets. Combustion analysis measurements were collected using a PerkinElmer 2400 Series II CHN Elemental Analyzer by facility staff.

2. Synthetic Details

(1) Fong, H.; Moret, M.-E.; Peters, J. C. *Organometallics* **2013**, *32*, 3053.
(2) Stoll, S.; Schweiger, A. *J. Magn. Reson.* **2006**, *178*, 42.

[P_3^B(μ-H)Fe(H)(CO)][K_2(THF)$_n$] 2: A bright yellow THF solution of P_3^B(μ-H)Fe(H)(CO) **1** (18.2 mg, 26.9 μmol) was stirred over an excess of K metal for 2 h becoming very dark red-brown. The solution was decanted away from the K and the solvent was removed. The resulting dark residue was washed with pentane and extracted with THF. The solvent was removed and triturated with Et_2O, yielding the product as a dark powder (17.1 mg). X-Ray quality crystals were grown by vapor diffusion of pentane into a THF/benzene (2:1) solution of the complex. Additional characterization and reactivity studies were carried out with *in situ* generation of this complex (>90% yield by NMR versus PPh_3 internal standard; Mössbauer spectroscopy) because of its facile oxidation. The compound was observed to be stable in sealed solutions over time (J. Young tube; monitored by NMR), but decomposed when attempts were made to store the complex in the glovebox under a nominally inert atmosphere as a solid, even at low temperatures (-35 °C). $^{31}P\{^1H\}$ NMR (THF/C_6D_6; 162 MHz): δ 102.3 (2P), -1.5 (1P). ^1H NMR (THF-d_8; 400 MHz): δ 7.85-7.75 (overlapping m, 3H), 7.25-7.4 (overlapping m, 3H), 7.00-6.75 (overlapping m, 6H), 2.48 (^{i}Pr C*H*, br, 2H) 2.43 (^{i}Pr C*H*, br, 2H), 1.90 (^{i}Pr C*H*, septd, *J* = 7, 2.3 Hz, 2H) 1.45-0.8 (^{i}Pr CH_3, 36H), -19.12 (B-*H*-Fe, br, 1H), -20.76 (Fe-*H*, t, *J* = 65 Hz, 1H). $^{11}B\{^1H\}$ NMR (THF-d_8; 128 MHz): δ 2.0. $^{13}C\{^1H\}$ NMR (THF/C_6D_6; 101 MHz; ^{13}CO-labeled): δ 230.7 (br). IR of [P_3^B(μ-H)Fe(H)(^{12}CO)][K_2(THF)$_n$] (thin film, cm^{-1}) : ν_{CO} = 1575; $\nu_{Fe\text{-}H}$ = 1760, 1824. IR of [P_3^B(μ-H)Fe(H)(^{13}CO)][K_2(THF)$_n$] (thin film, cm^{-1}) : ν_{CO} = 1538. Mössbauer (80 K; frozen THF solution, mm/s): δ = 0.09; ΔE_Q = 2.39.

[P_3^B(μ-H)Fe(H_2)(CO)][K(THF)$_n$] 3: A solution of dianionic **2** in THF was generated *in situ* and transferred to a J. Young NMR tube. Concurrently, a stream of wet, O_2-free N_2 was prepared by bubbling N_2 through water over several hours. The headspace of the reaction vessel was evacuated and backfilled with wet N_2 and thoroughly mixed. This process was repeated iteratively (~5x) until the reaction underwent a dramatic color change from very dark red-brown to yellow-orange. This resulted in quantitative conversion to the trihydride complex **3** as judged by NMR spectroscopy (versus PPh_3 internal standard). Clean isolation of this species was complicated by its tendency to reductively eliminate H_2, yielding **4**. X-Ray quality crystals could be grown by slow evaporation of an Et_2O solution of the complex in a sealed vessel containing HMDSO. $^{31}P\{^1H\}$ NMR (THF-d_8; 162 MHz): δ 106.72 (m, 2P), -9.64 (1P). ^1H NMR (THF-d_8; 400 MHz): 7.31 (Ar C-*H*, 2H), 7.26 (Ar C-*H*, 2H), 7.17 (Ar C-*H*, d, *J* = 7.4 Hz, 1H), 6.79 (Ar C-*H*, overlapping, 5H), 6.64 (Ar C-*H*, t, *J* = 7.3 Hz, 1H), 6.51 (Ar C-*H*, br, 1H), 2.53 (PC-*H*, br, 4H), 1.58 (PC-*H*, br, 2H), 1.31 (CH_3, dd, *J* = 12, 6.7 Hz, 6H), 1.13 (CH_3, dq, *J* = 27, 6.6 Hz, 12H), 0.96 (CH_3, dd, *J* = 12, 6.8 Hz, 6H), 0.67 (CH_3, ddd, *J* = 19.4, 12.5, 6.9 Hz, 12H), -8.40 (Fe-*H*, td, *J* = 66, 16 Hz, 1H), -14.69 (Fe-*H*-B, br, 1H), -20.53 (t, *J* = 48 Hz, 1H). ^{11}B NMR (THF; 128 MHz): δ -4.15. $^{13}C\{^1H\}$ NMR (THF; 101 Mz; ^{13}CO-labeled): 225.3 (m). IR of [P_3^B(μ-H)Fe(H_2)(^{12}CO)][K(THF)$_n$] (thin film, cm^{-1}): ν_{CO} = 1787; $\nu_{Fe\text{-}H}$ = 1826, 1862. IR of [P_3^B(μ-H)Fe(H_2)(^{13}CO)][K(THF)$_n$] (thin film, cm^{-1}): ν_{CO} = 1748.

[P_3^BFe(H)(CO)][K(THF)$_n$] 4: A solution of **2** was generated *in situ* from **1** (74 mg, 0.109 mmol) and transferred to a Schlenk tube. From this mixture, **3** was generated (*vide supra*), the solution was frozen, the headspace was evacuated and the mixture was stirred at room temperature for 36 h, resulting in the conversion of **3** to **4** with loss of H_2. The solution was filtered through Celite, the solvent was removed *in vacuo*, and the residue was extracted with THF. The solvent was again removed and the residue was washed with benzene and then extracted with THF, yielding the product as an orange-yellow powder after the THF was removed (82.5 mg, 81% yield). X-

Ray quality crystals were grown by vapor diffusion of pentane into a THF/benzene solution of the complex. $^{31}P\{^{1}H\}$ NMR (THF-d_8; 162 MHz): δ 90.7. ^{1}H NMR (THF-d_8; 400 MHz): δ 7.25 (d, J = 7.4 Hz, 3H), 7.01 (d, J = 7.3 Hz, 3H), 6.68 (t, J = 7.1 Hz, 3H), 6.51 (t, J = 7.1 Hz, 3H), 2.15 (br, 3H), 2.27 (br, 6H), 0.99 (br, 18H), 0.81 (br, 18H) -13.93 (qd, J = 47, 7.2 Hz, 1H). $^{11}B\{^{1}H\}$ NMR (THF-d_8; 128 MHz): δ 12.9. $^{13}C\{^{1}H\}$ NMR (THF-d_8; 101 MHz; ^{13}CO-labeled): δ 222.2 (m). UV/Vis (THF, nm {M^{-1} cm^{-1}}): 407 {sh}, 344 {8500}. IR of $[P_3^BFe(H)(^{12}CO)][K(THF)_n]$ (thin film, cm^{-1}): ν_{CO} = 1754. IR of $[P_3^BFe(H)(^{13}CO)][K(THF)_n]$ (thin film, cm^{-1}): ν_{CO} = 1705. Mössbauer (80 K; 2-MeTHF/C_6H_6 solution, mm/s): δ = 0.03; ΔE_Q = 1.28.

$(P_3^B$-H)Fe(CO) 5: 4 (64.9 mg, .076 mmol) was dissolved in THF (4 mL) and cooled to -78 °C. The solution was added to a similarly chilled THF (2 mL) suspension of $[Cp_2Co][PF_6]$ (30.3 mg, .0901 mmol). The mixture was stirred at -78 °C for 5 min, turning red-brown, then at room temperature for an additional 30 min. The solution was filtered, the solvent was removed *in vacuo,* and the resulting brown powder was triturated with Et_2O (5 mL). The product was washed with pentane (3 mL) and then extracted with benzene (5 mL). Lyophilization yielded the product as a brown powder (38.9 mg, 78%). X-Ray quality crystals were grown by slow evaporation of an Et_2O solution of the complex. ^{1}H NMR (C_6D_6; 300 MHz): 13.9, 8.9, 7.4, 5.6, 4.2, 1.3, -0.2. UV/Vis (THF, nm {M^{-1} cm^{-1}}): 865 {300}, 575 {sh}, 495 {800}. Solution magnetic moment (Evans Method; 25 °C): 1.9μ_B. IR of (P_3^B-H)Fe(CO) (thin film, cm^{-1}): ν_{CO} = 1862 cm^{-1}; $\nu_{B\text{-}H}$ = 2588 cm^{-1}. Anal. Calcd for $C_{37}H_{55}BFeOP_3$: C, 65.80; H, 8.21; N, 0.00. Found: C, 65.45; H, 8.53; N, <0.02. Mössbauer (80 K, frozen benzene solution, 50 mT, mm/s): δ = 0.22; ΔE_Q = 0.43.

P_3^BFe(CH_2OTMS) 6: A THF solution of the dianionic complex **2** was generated *in situ* from **1** (20.3 mg) and cooled to -78 °C. A slight excess of Me_3SiOTf (16 μL; 2.5 equiv) was added. The reaction mixture was stirred at -78 °C for 15 min then at room temperature for 15 min. The solvent was removed *in vacuo* and the product was extracted with pentane and filtered through Celite. The solvent was removed and the residue was dissolved in benzene and lyophilized to yield the product mixture as a dark orange/brown powder (19.5 mg; ~80% **6** as determined by Mössbauer spectroscopy). All reactivity studies and characterization were carried out using this product mixture, which has doublet impurities including **5**. X-Ray quality crystals were grown by cooling a saturated Et_2O/MeCN solution at -30 °C. ^{1}H NMR (C_6D_6; 400 MHz): δ 59.5, 30.1, 21.7, 17.6, 7.8, 5.8, 4.8, -3.1, -3.3, -4.4, -15.2. Solution magnetic moment (Evans Method; 25 °C; ~80% **6**, 20% low-spin (1/2) impurity): 3.44μ_B. Mössbauer (80 K, frozen benzene solution, mm/s): δ = 0.49; ΔE_Q = 2.05.

Reaction of 6 with H_2: A solution of **6** (10-20 mg) was prepared in C_6D_6. In a J. Young NMR tube, the solution was frozen and the headspace was evacuated and backfilled with H_2. The solution was mixed at room temperature until full conversion of the starting material was observed by NMR spectroscopy (~24 h). From these mixtures, the volatiles were vacuum transferred into a second J. Young NMR tube containing a stock solution of ferrocene as an internal standard and the yield of CH_3OSiMe_3 was determined (55%, 50%, 46%; 50% average; assumes starting material **6** is 80% clean). The identity of the product was confirmed by comparison to an authentic sample.

Reaction of 6 with $PhSiH_3$: A solution of **6** (10-20 mg) was prepared in C_6D_6. This solution was added to a J. Young NMR tube with excess $PhSiH_3$ (5 equiv) and a stock solution of ferrocene as an NMR standard. The resulting solution was mixed at room temperature until full conversion of the starting material was observed and the yield of $PhSiH_2CH_2OSiMe_3$ was determined by integration versus a ferrocene internal standard (36%, 45%, 58%; 47% average; assumes starting material **6** is 80% clean). Vacuum transfer of this compound was not found to be reliable for quantification. The product of this reaction was assigned on the basis of NMR spectroscopy with comparison to a similar species reported by Hill and coworkers (*Angew. Chem. Int. Ed.* **2015**, *54*, 10009.). ^{1}H NMR (C_6D_6; 400 MHz): δ 4.57 (SiH_2, t, J = 3 Hz, 2H), 3.56 (CH_2, t, J = 3 Hz, 2H), 0.05 (Si(CH_3)$_3$, s, 9H). Aromatic C-H resonances in the ^{1}H NMR overlap with $PhSiH_3$ resonances, which is present in excess. ^{13}C{^{1}H} NMR (C_6D_6; 101 MHz; ^{13}C-labeled): δ 50.42 (Si-CH$_2$O).

Rate comparison for the reaction of 6 with H_2/D_2: A stock solution of **6** was prepared in C_6D_6 and equal volumes of the solution were added to two separate J. Young NMR tubes. The tubes were degassed by two freeze-pump-thaw cycles, frozen, and the headspace was backfilled with either an atmosphere of H_2 or an atmosphere of D_2. The solutions were thawed and mixed at room temperature, proceeding partially to completion as observed by NMR spectroscopy. In either case, the resulting solution was frozen, the headspace was evacuated, and the volatiles were vacuum transferred into a second J. Young NMR tube containing a stock solution of Fc as an internal standard (50 μL; 0.1 M in C_6D_6). Comparison of the relative product yields is consistent with a normal KIE with an average of 1.25 over two runs (individual runs: 1.16, 1.35).

3. NMR Spectra

$[P_3^B(\mu\text{-H})Fe(H)(CO)][K_2(THF)_n]$ 2:

Figure S3.1: ^{1}H NMR (400 MHz) spectrum of **2** in THF-d_8.

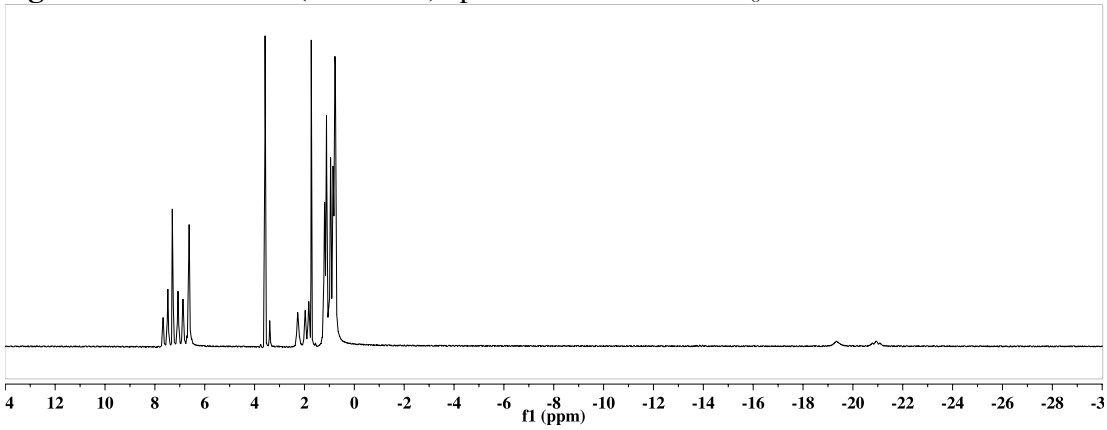

Figure S3.2: $^{31}P\{^{1}H\}$ NMR (162 MHz) spectrum of **2** in THF-d_8.

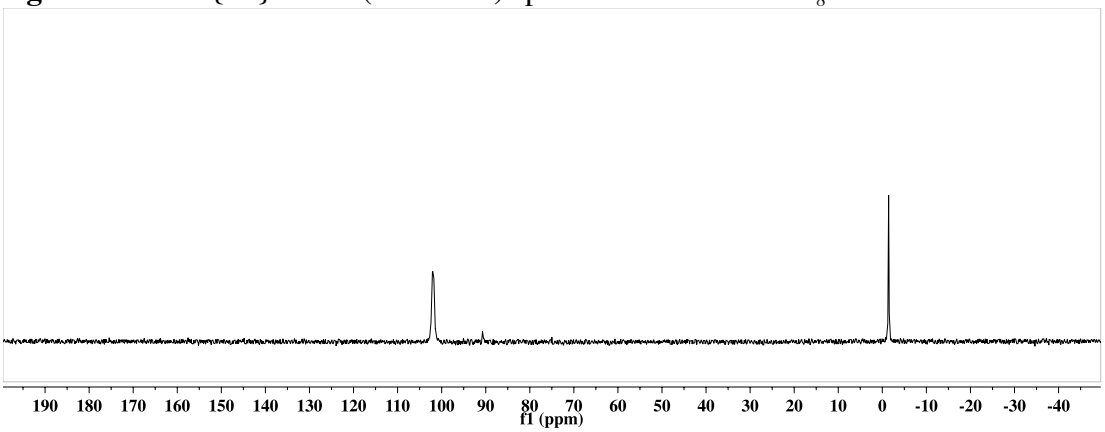

Figure S3.3: $^{11}B\{^{1}H\}$ NMR (128 MHz) spectrum of **2** in THF-d_8.

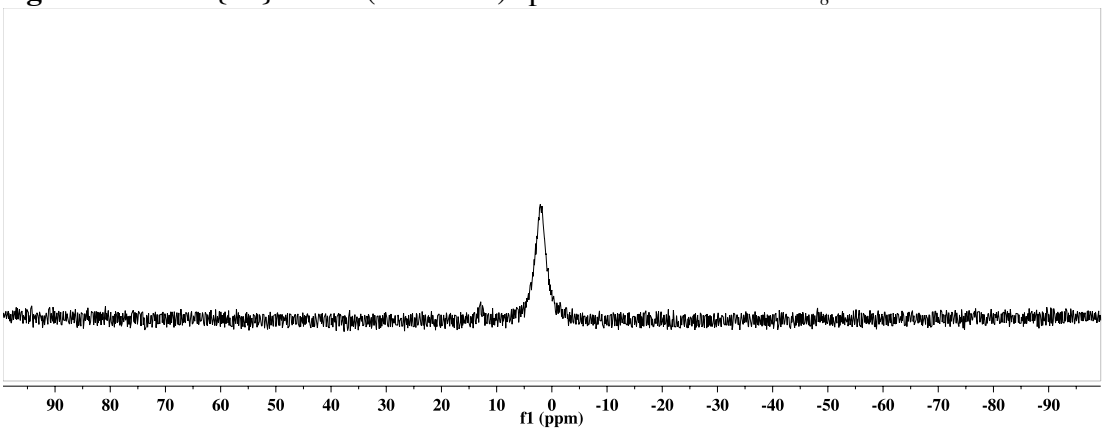

Figure S3.4: $^{13}C\{^{1}H\}$ NMR (101 MHz; ^{13}CO-labeled) spectrum of **2** in a mixture of THF and C_6D_6.

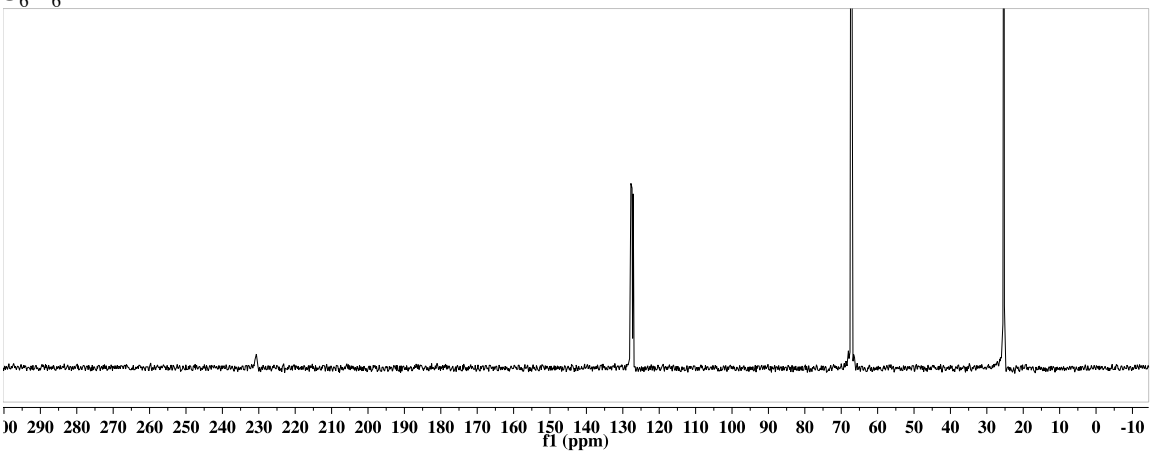

$[P_3^B(\mu\text{-}H)Fe(H)_2(CO)][K(THF)_n]$ 3:

Figure S3.5: ^{1}H NMR (400 MHz) spectrum of **3** in THF-d_8.

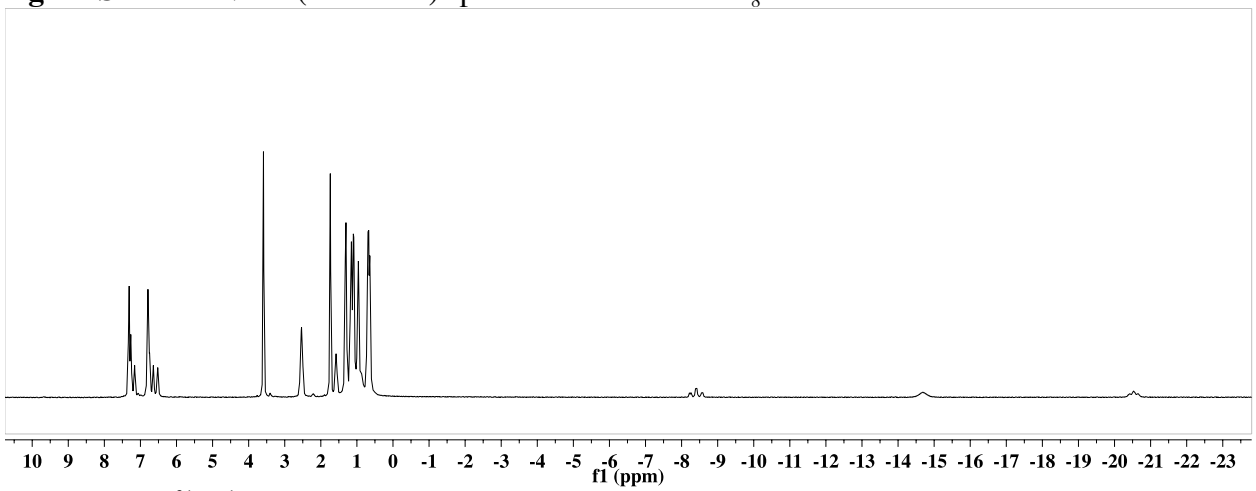

Figure S3.6: $^{31}P\{^1H\}$ NMR (162 MHz) spectrum of **3** in THF-d_8.

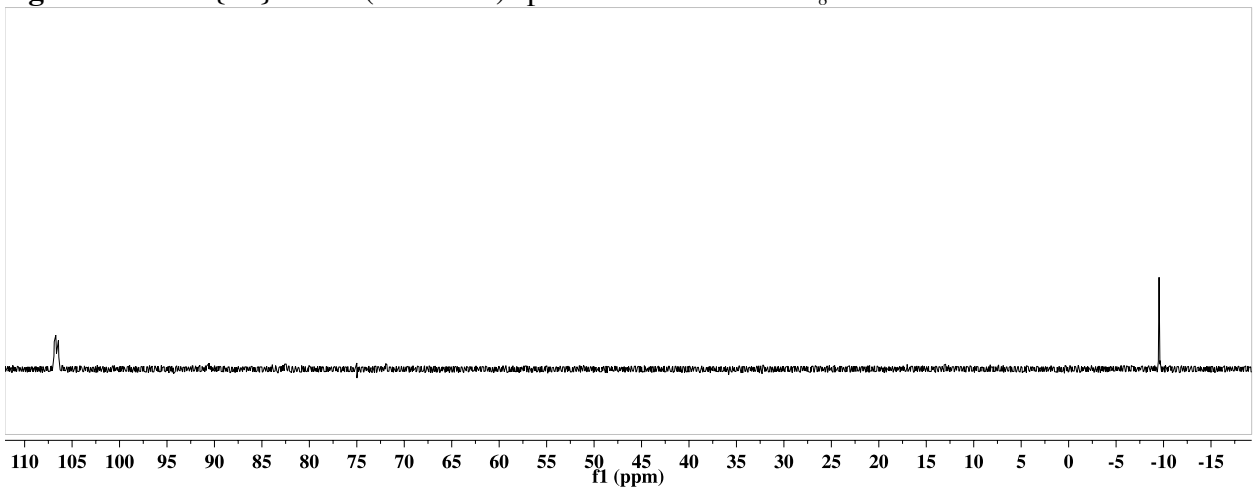

Figure S3.7: $^{11}B\{^1H\}$ NMR (128 MHz) spectrum of **3** in THF.

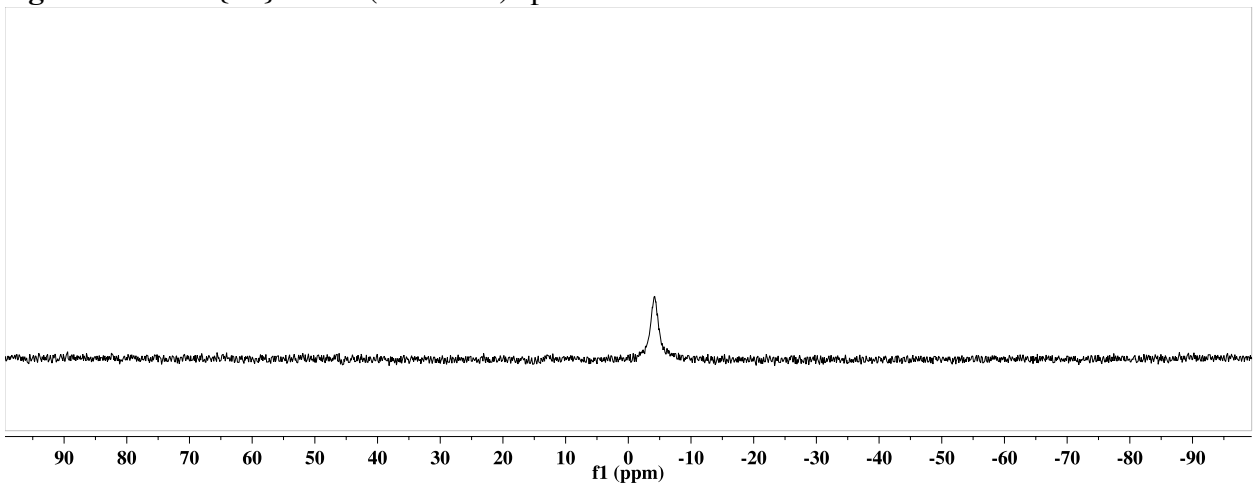

Figure S3.8: $^{13}C\{^{1}H\}$ NMR (101 MHz; ^{13}CO-labeled) spectrum of **3** in THF.

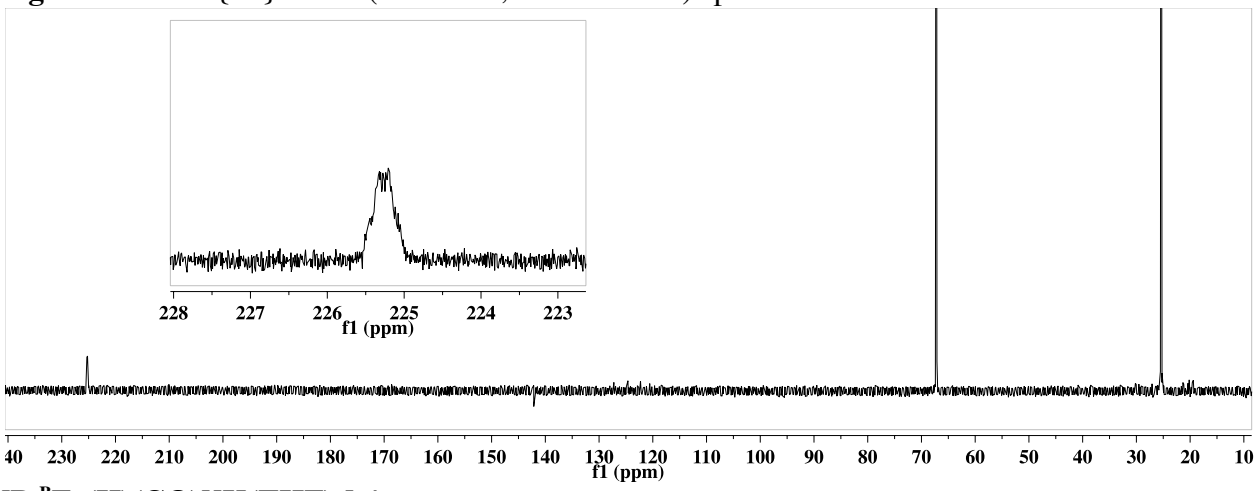

$[P_3^BFe(H)(CO)][K(THF)_n]$ 4:

Figure S3.9: ^{1}H NMR (400 MHz) spectrum of **4** in THF-d_8.

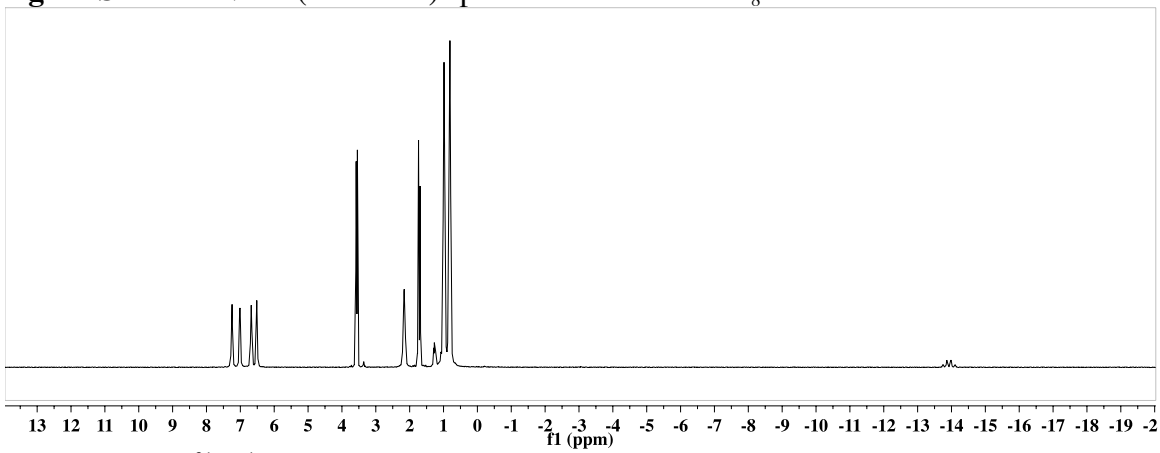

Figure S3.10: $^{31}P\{^{1}H\}$ NMR (162 MHz) spectrum of **4** in THF-d_8. Solution symmetry has been observed in isoelectronic Rh and Ir complexes at room temperature by Nakazawa and coworkers (*Organometallics* **2012**, *31*, 3155. *Organometallics* **2012**, *31*, 4251.)

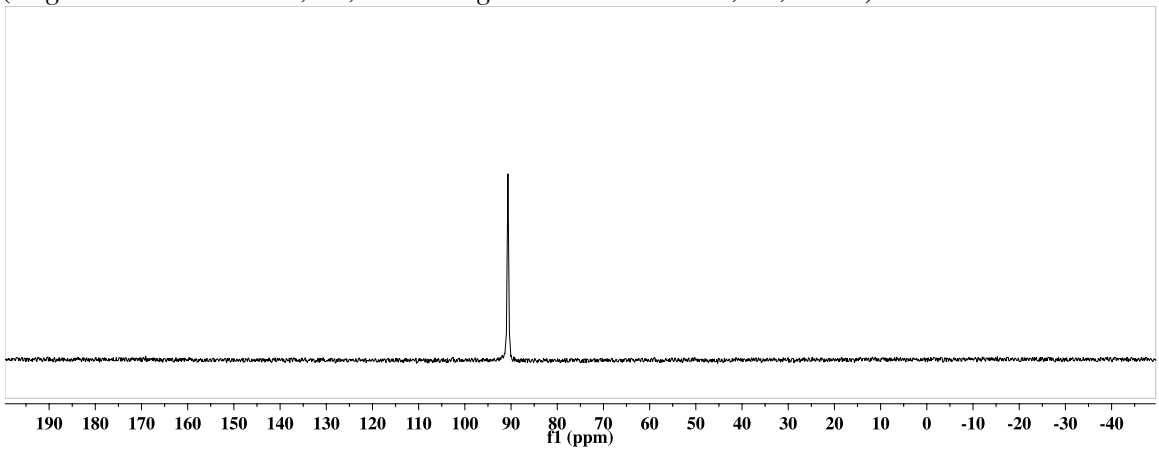

Figure S3.11: $^{31}P\{^{1}H\}$ NMR (202 MHz) spectrum of **4** in THF-d_8 collected at -80 °C.

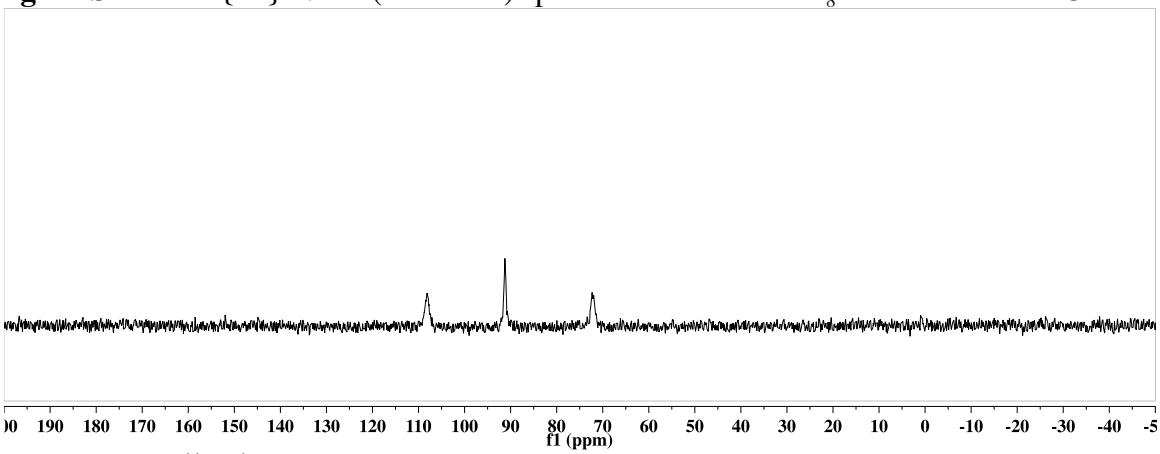

Figure S3.12: $^{11}B\{^{1}H\}$ NMR (128 MHz) spectrum of **4** in THF-d_8.

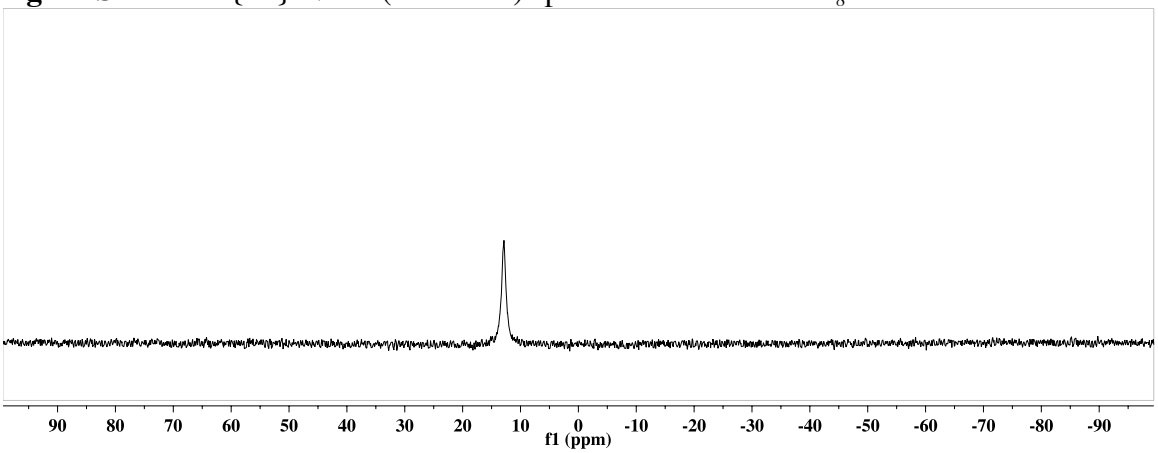

Figure S3.13: $^{13}C\{^{1}H\}$ NMR (101 MHz; ^{13}CO-labeled) spectrum of **4** in THF-d_8.

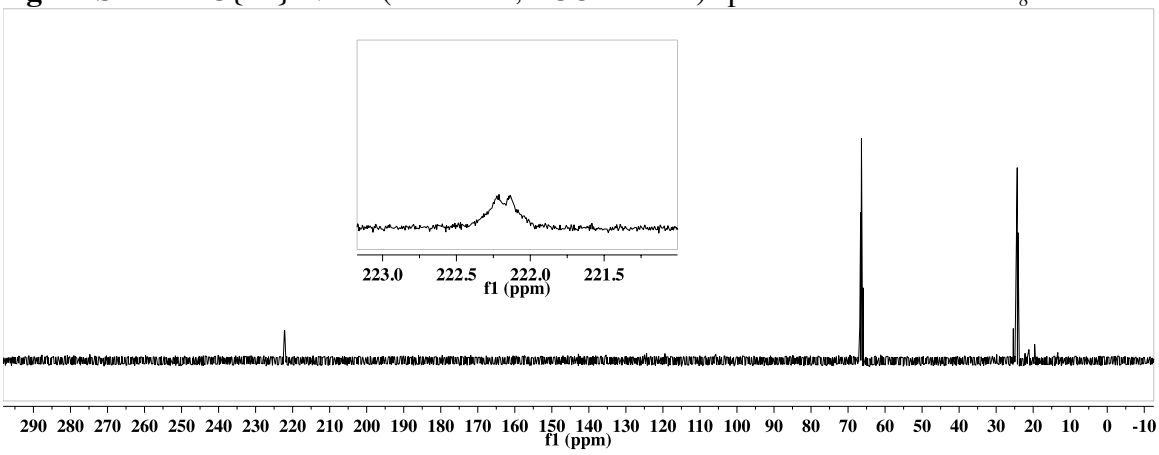

$(P_3^B$-H)Fe(CO) 5:

Figure S3.14: ^{1}H NMR (300 MHz) spectrum of **5** in C_6D_6 (Et_2O impurity observable).

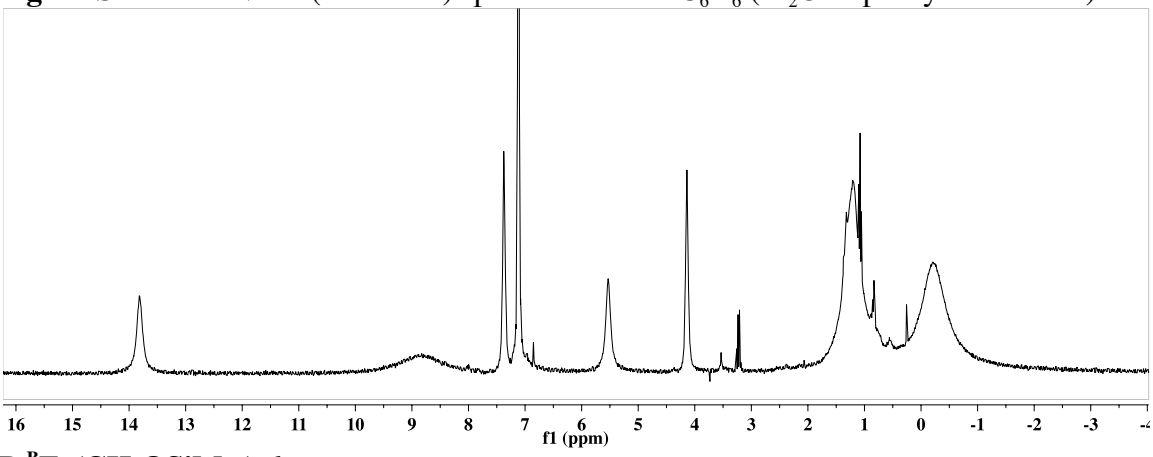

P_3^BFe(CH_2OSiMe_3) 6:

Figure S3.15: ^{1}H NMR (400 MHz) spectrum of **6** in C_6D_6.

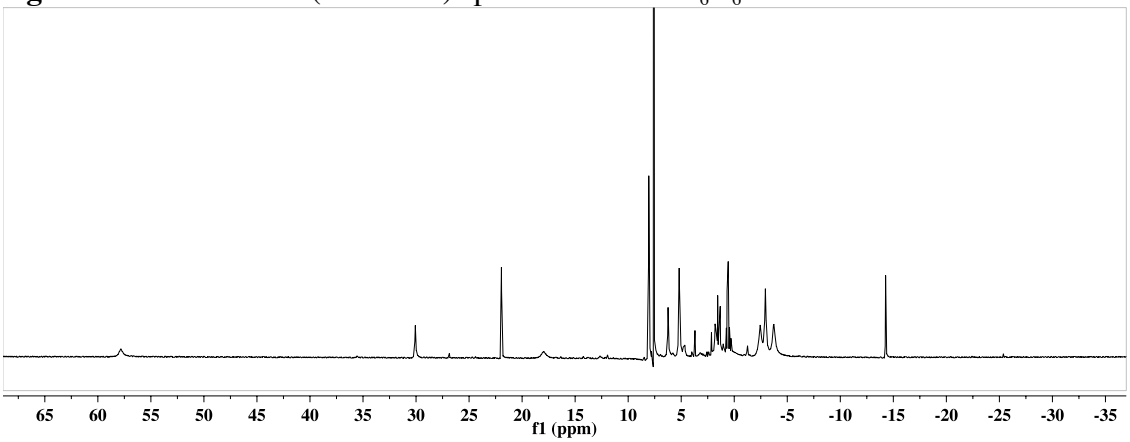

Figure S3.16: ^{1}H NMR (400 MHz) spectrum of the product mixture generated from the reaction of **6** with $PhSiH_3$. Additional, paramagnetically shifted resonances associated with the Fe-containing products are observable with a wider spectrum window.

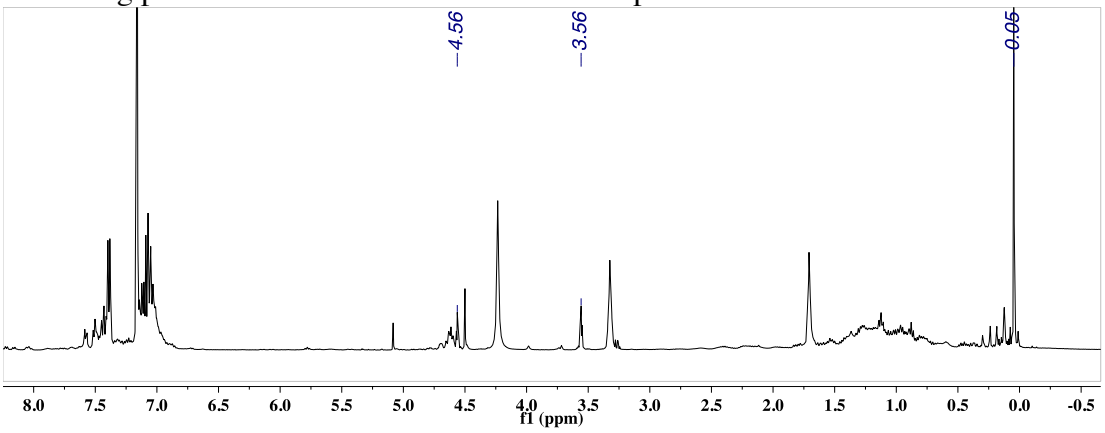

Figure S3.17: ^{1}H NMR (400 MHz) spectrum of the product mixture generated from the reaction of **6** with $PhSiH_3$ with isolation from iron-containing products *via* vacuum transfer.

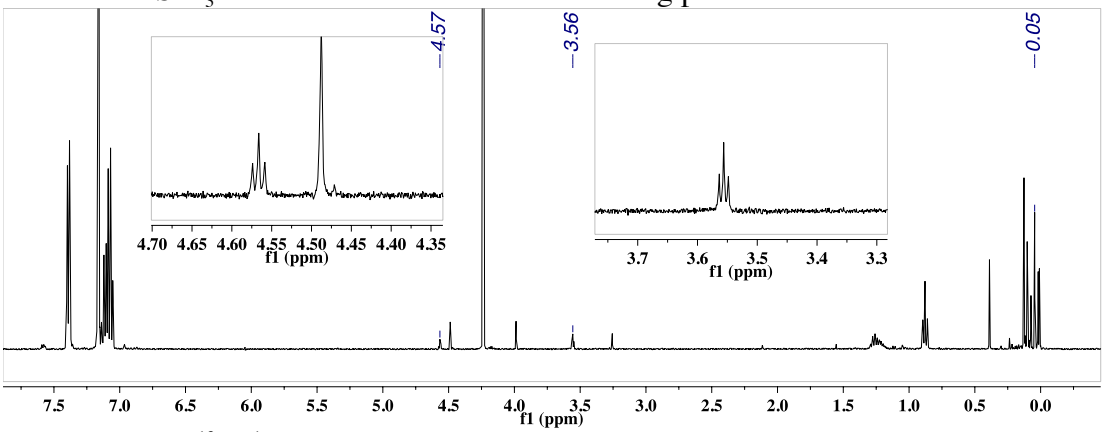

Figure S3.18: $^{13}C\{^{1}H\}$ NMR (101 MHz) spectrum of the product mixture generated from the reaction of **6-^{13}CO** with $PhSiH_3$.

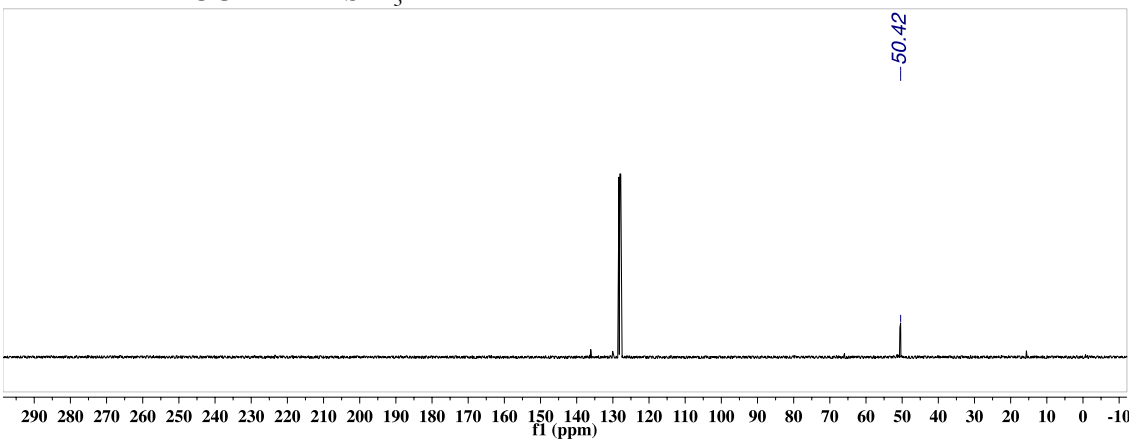

4. IR Spectra

Figure S4.1: Thin film IR spectrum of **2**.

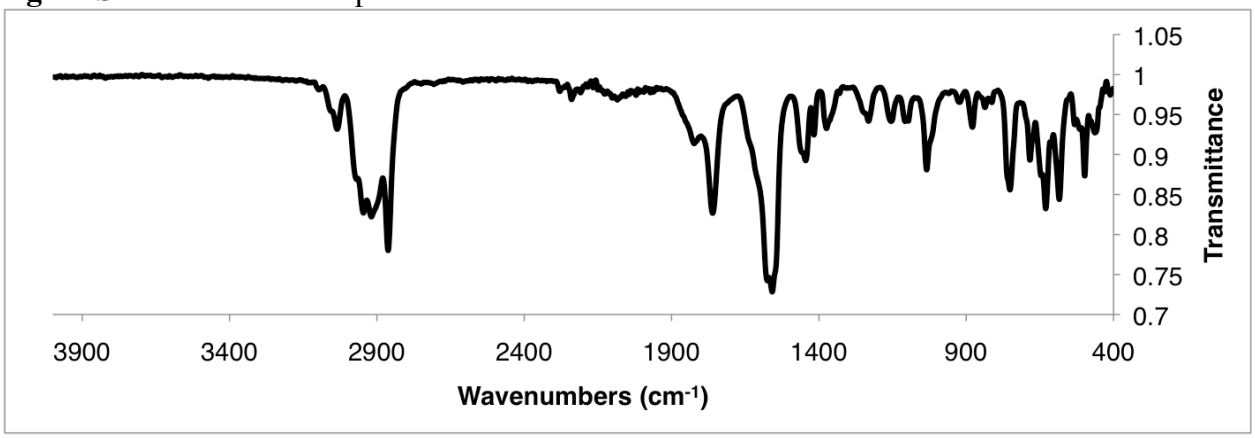

Figure S4.2: Thin film IR spectrum of **3**.

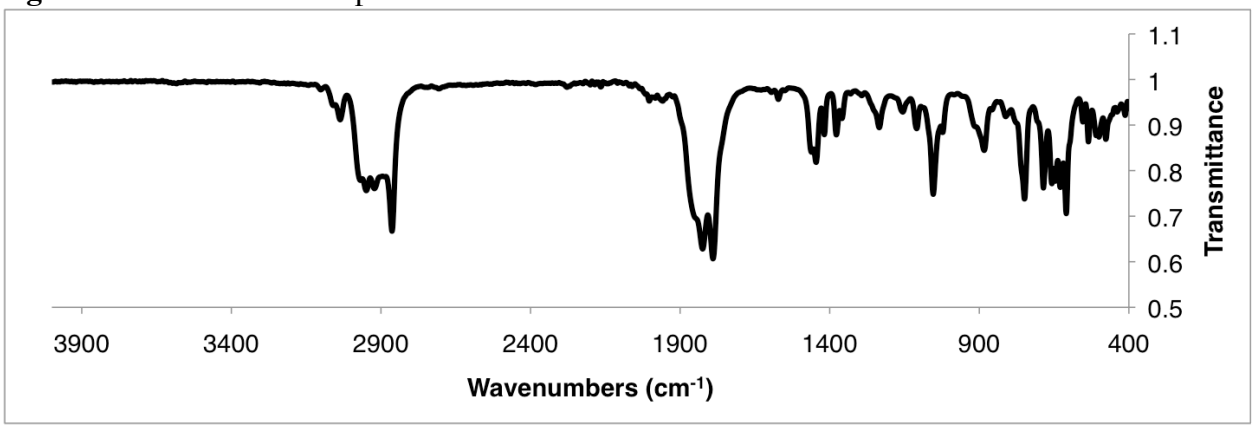

Figure S4.3: Thin film IR spectrum of **4**.

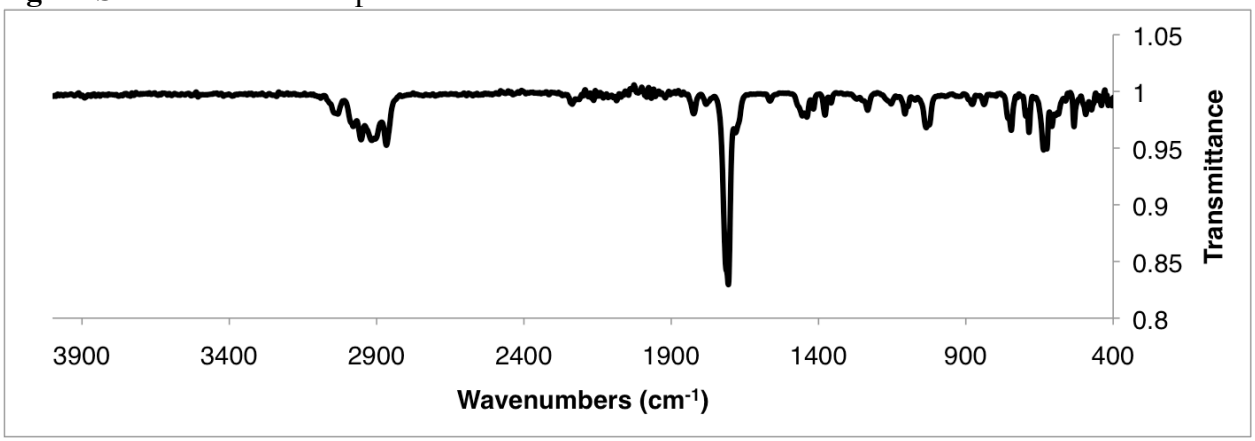

Figure S4.4: Thin film IR spectrum of **5**.

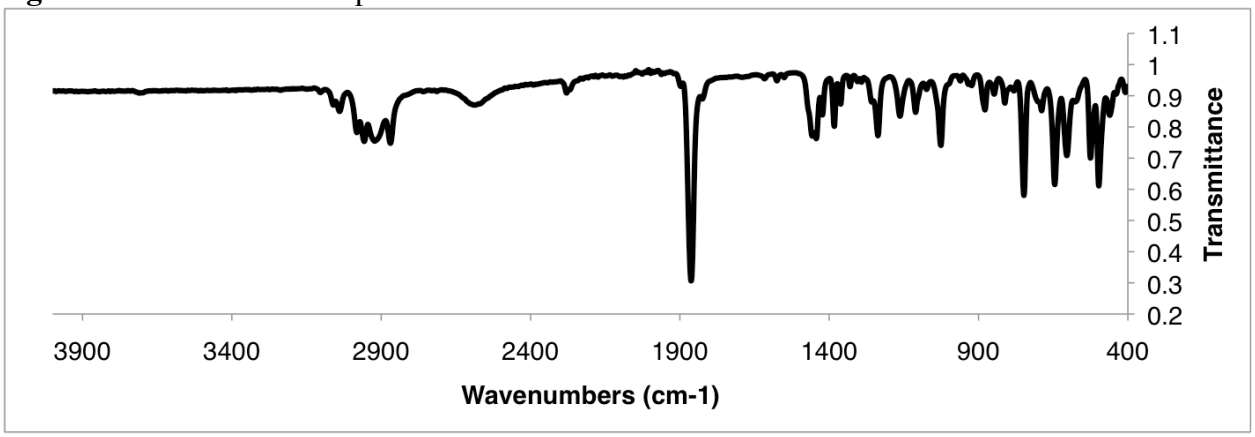

5. UV-Vis Spectra in THF at 298 K

Figure S5.1: UV-Vis Spectrum of **2** in THF.

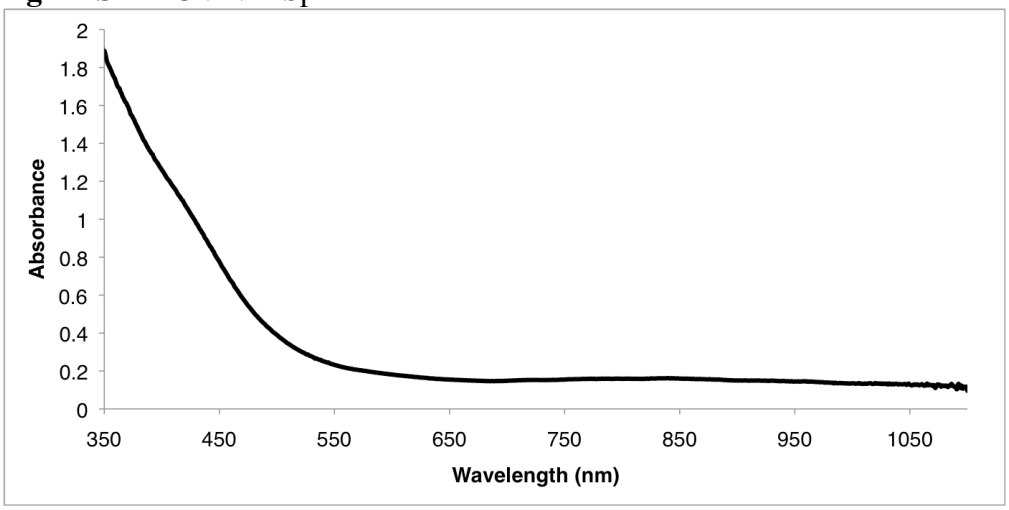

Figure S5.2: UV-Vis Spectrum of **4** in THF.

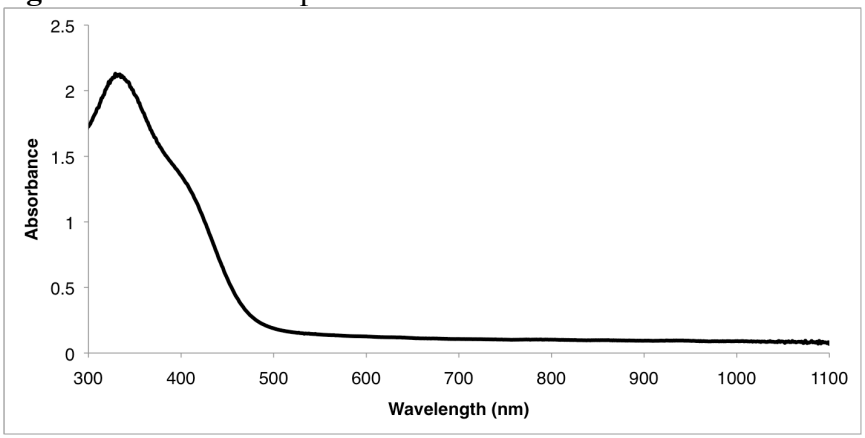

Figure S5.3: UV-Vis Spectrum of **5** in THF.

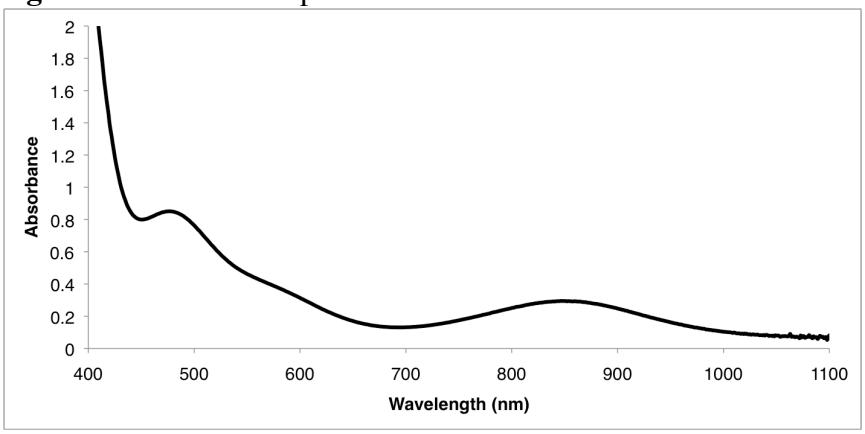

6. EPR Spectra

Figure S6.1: X-Band EPR Spectrum of **5** collected at 77K in a 2-MeTHF glass. Simulation parameters: g = [2.4 2.0322 2.0322]; lw = 5; HStrain = [300 200 175]

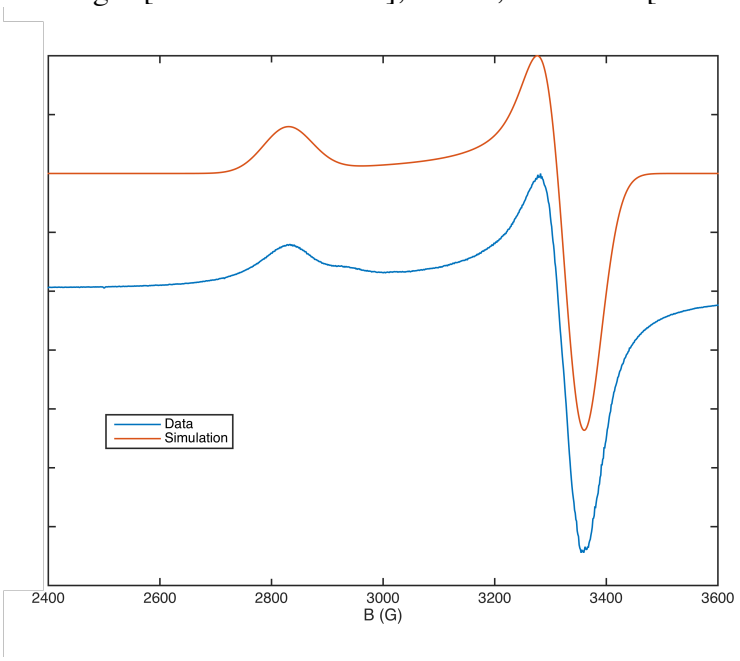

7. Mössbauer Spectra

Figure S7.1: Spectrum of **1** collected at 80 K in benzene ($\delta = 0.01$; $\Delta E_Q = 1.09$).

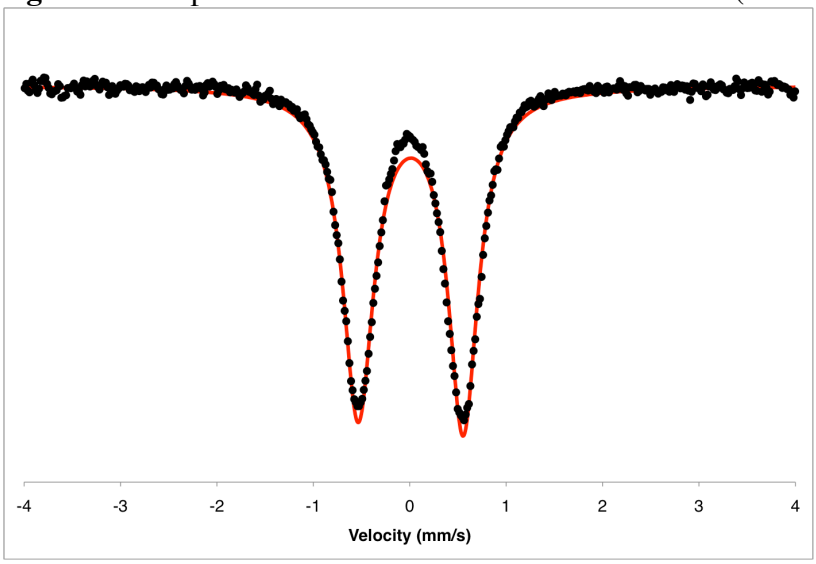

Figure S7.2: Spectrum of **2** collected at 80 K in THF ($\delta = 0.09$; $\Delta E_Q = 2.39$).

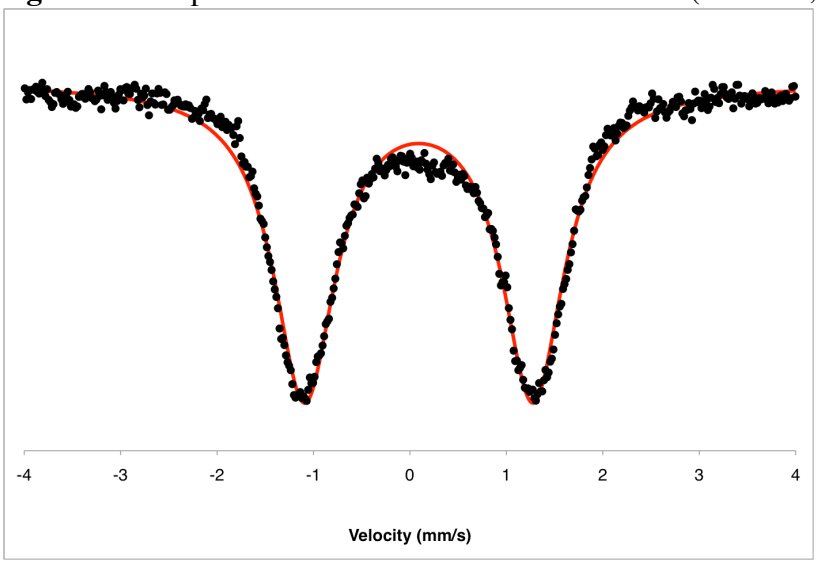

Figure S7.3: Spectrum of **4** collected at 80 K in a 2-MeTHF/benzene mixture ($\delta = 0.03$; $\Delta E_Q = 1.28$). Residual signal is consistent with the presence of a minor amount of **5** generated from oxidation during sample handling ($\delta = 0.19$; $\Delta E_Q = 0.47$).

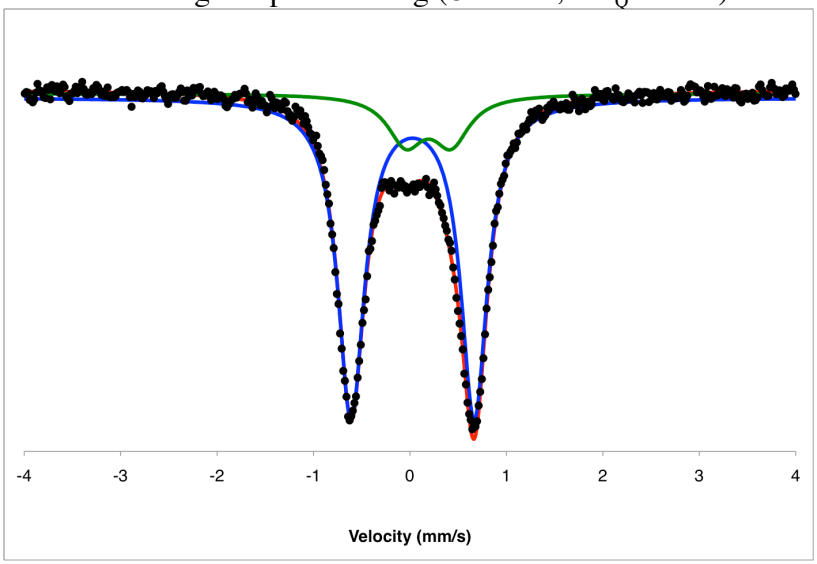

Figure S7.4: Spectrum of **5** collected at 80 K in frozen benzene with an applied 50 mT magnetic field ($\delta = 0.21$; $\Delta E_Q = 0.45$).

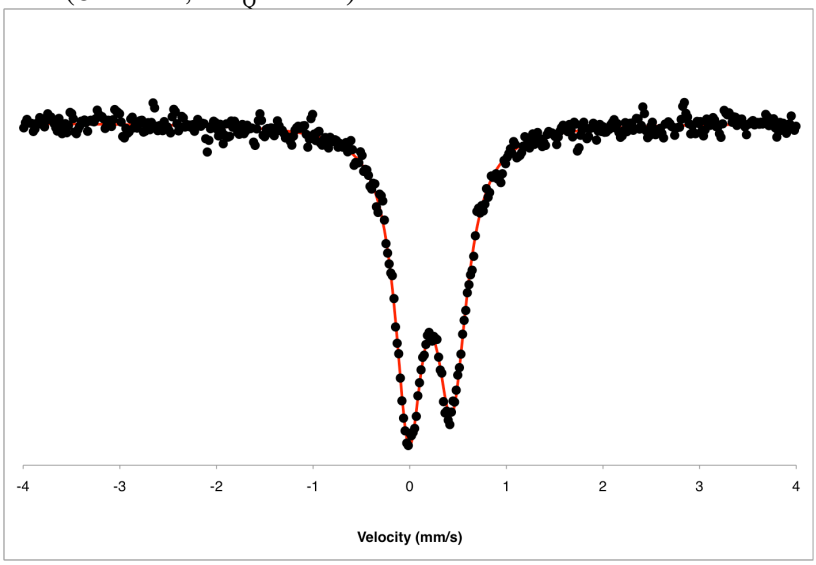

Figure S7.5: Spectrum of **5** collected at 80 K in frozen benzene ($\delta = 0.22$; $\Delta E_Q = 0.43$). Spectra collected with and without the magnet for **5** were collected on the same sample for approximately the same period of time.

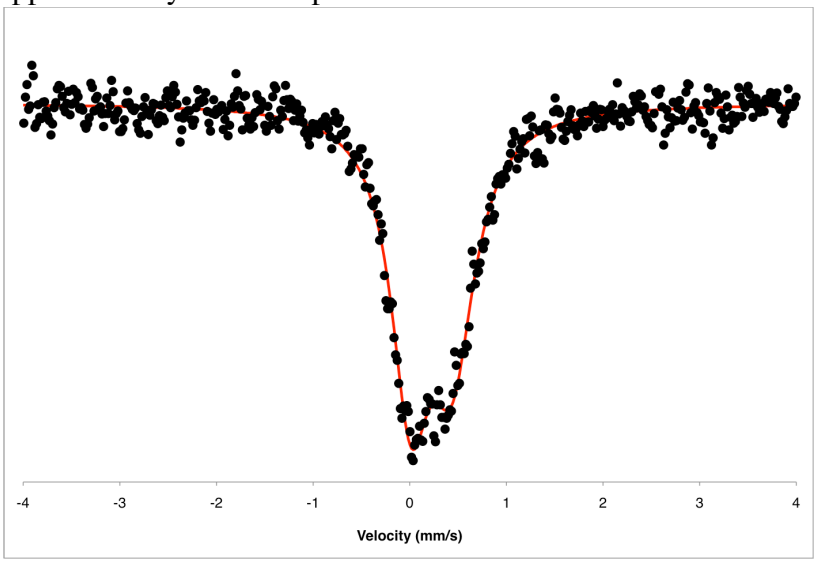

Figure S7.6: Spectrum of product mixture including **6** collected at 80 K in benzene) (δ = 0.49; ΔE_Q = 2.05; 78%). The minor component is likely representative of multiple species (δ = 0.19; ΔE_Q = 0.65; 22%).

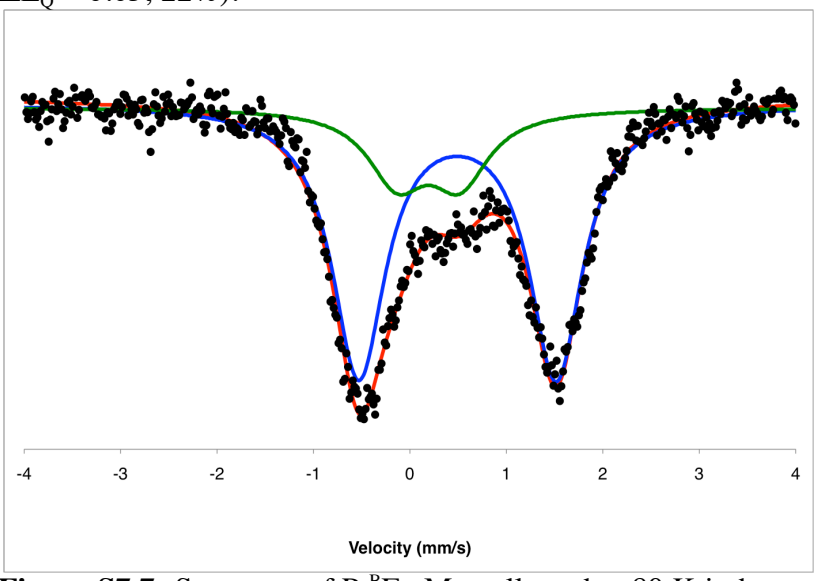

Figure S7.7: Spectrum of P_3^BFe-Me collected at 80 K in benzene (δ = 0.50; ΔE_Q = 1.84). Minor impurity: δ = 0.11; ΔE_Q = 0.28.

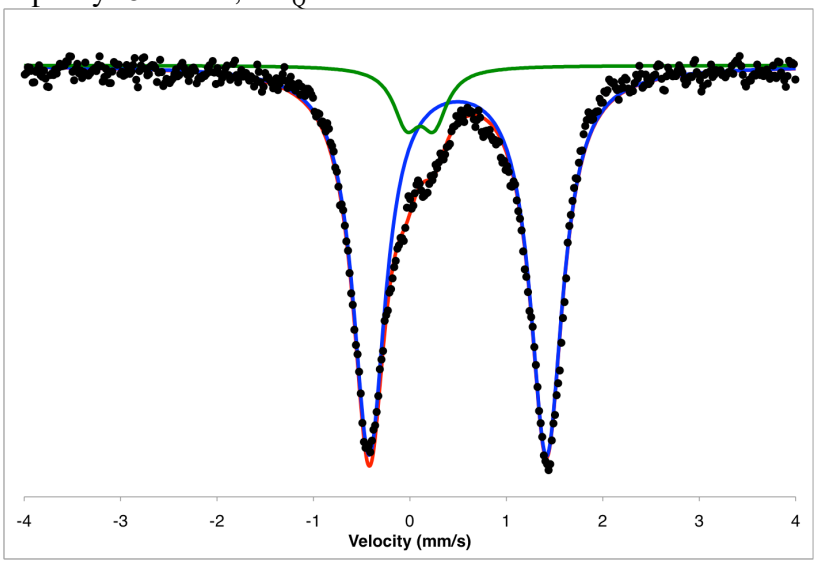

8. Labeling Experiments

For these experiments, $P_3^BFeCH_2OSiMe_3$ **6** was prepared from $P_3^B(\mu$-H)Fe(H)(CO) **2-H$_2$**, $P_3^B(\mu$-D)Fe(D)(CO) **2-D$_2$**, or a mixture of both. The isolated products (10-20 mg), **6-H$_2$**, **6-D$_2$**, or **6-H$_2$/D$_2$** were dissolved in C_6D_6 and treated with an atmosphere of H_2 or D_2 in a J. Young NMR tube. The solutions were mixed until full conversion of the starting material was observed (~24 h). Longer reaction times were not observed to change the product ratios or improve the yield of the CO-derived product. The resulting mixtures were vacuum transferred into a clean, dry J. Young tube and the product ratios were determined by ^{1}H NMR integration. Integrations relative to the *Me*$_3$Si- peak were used to determine the amount of fully deuterated product in the samples. A small amount of Et_2O was observed in one case, which overlapped with the product peak, so ^{13}C-labeled compounds were used to obtain improved integrations.

Figure S8.1: ^{1}H NMR (400 MHz) spectrum of the product mixture generated from the reaction of **6** with H_2 (with Fc internal standard).

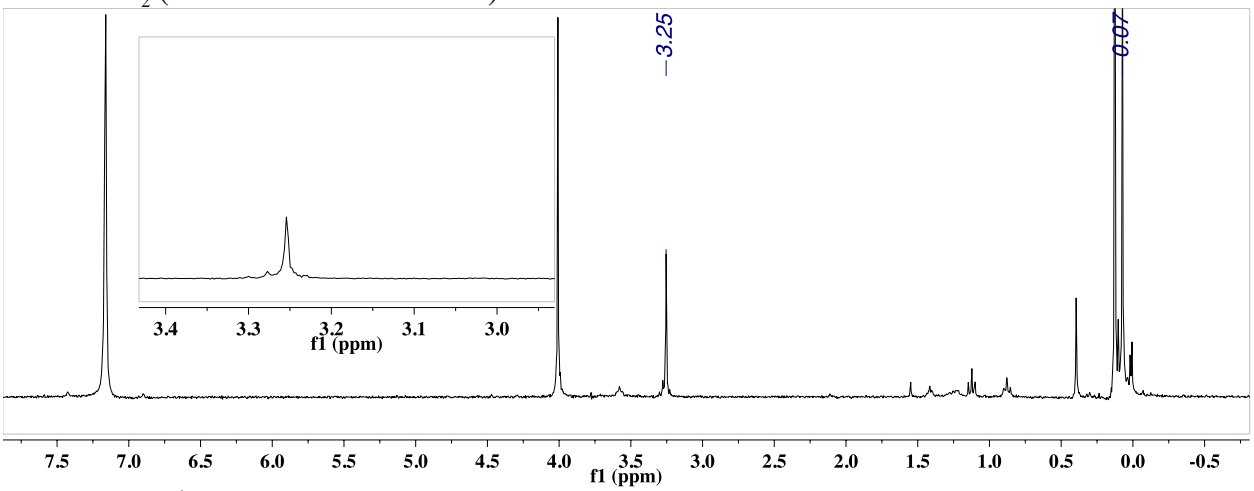

Figure S8.2: ^{1}H NMR (400 MHz) spectrum of the product mixture generated from the reaction of **6** with D_2.

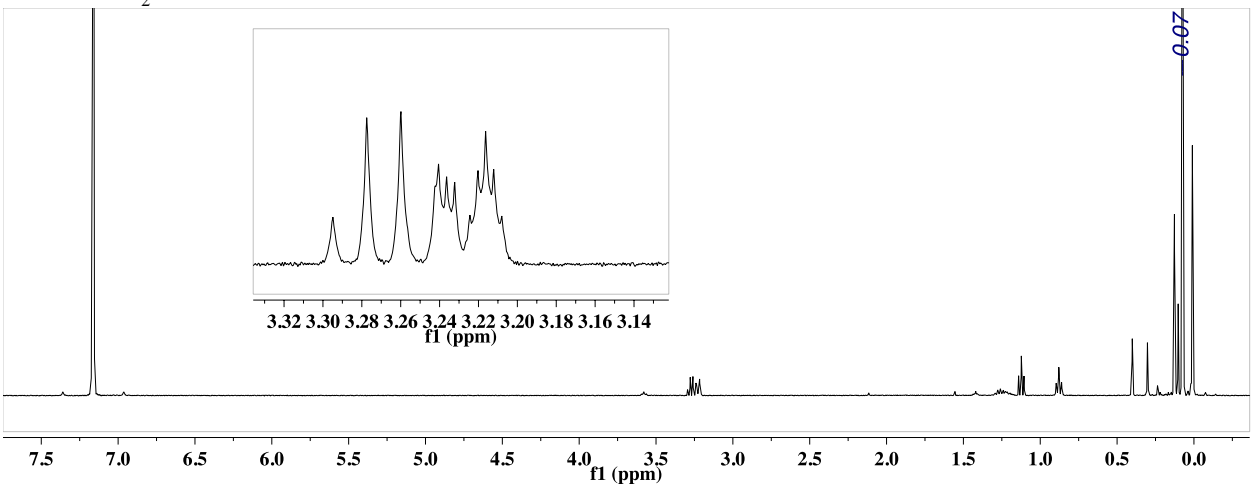

Figure S8.3: ^{1}H NMR (400 MHz) spectrum of the product mixture generated from the reaction of **6** with D_2 using ^{13}CO-labeled material.

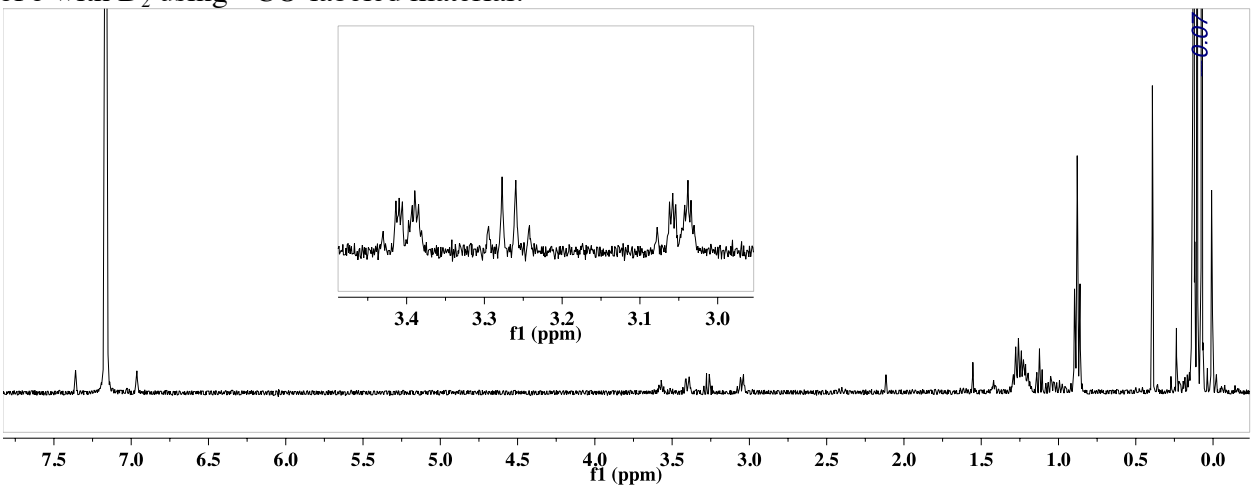

Figure S8.4: ^{1}H NMR (400 MHz) spectrum of the product mixture generated from the reaction of **6-D$_2$** with H_2

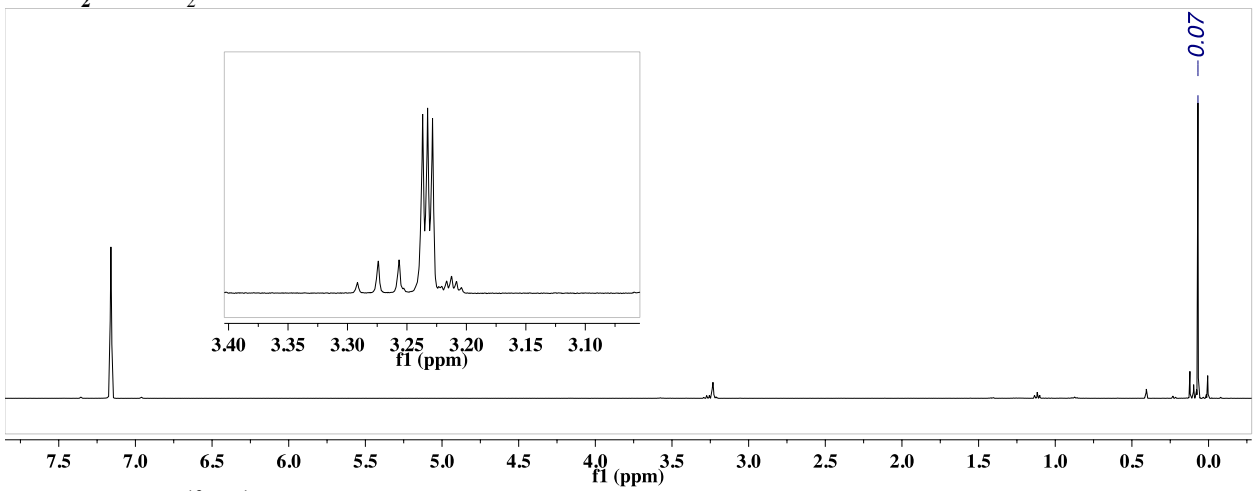

Figure S8.5: $^{13}C\{^{1}H\}$ NMR (101 MHz) spectrum of the product mixture generated from the reaction of **6-D$_2$** with H_2 using ^{13}CO-labeled material.

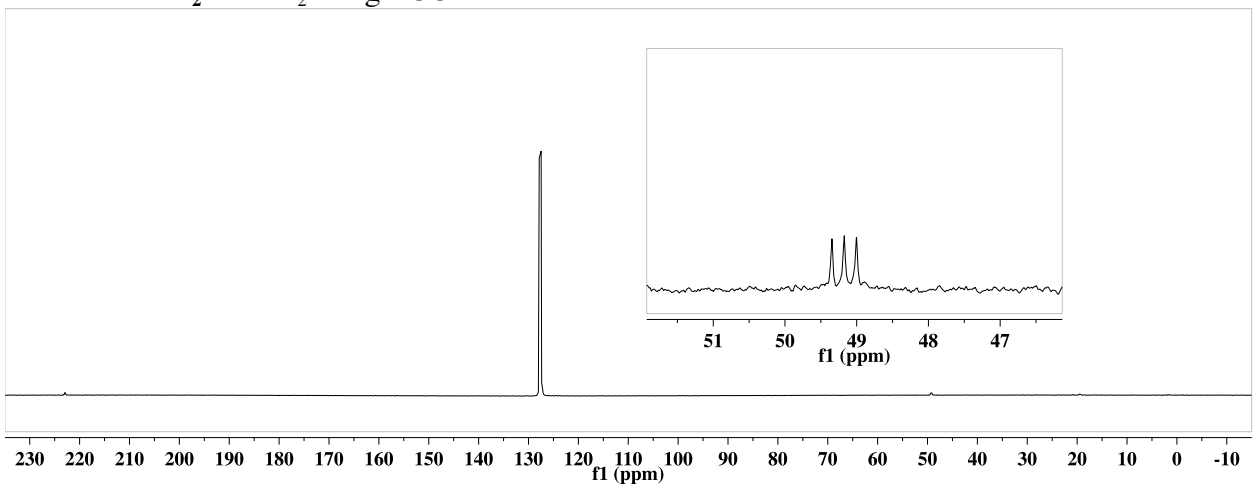

Figure S8.6: ^{1}H NMR (400 MHz) spectrum of the product mixture generated from the reaction of **6-D$_2$** with D_2

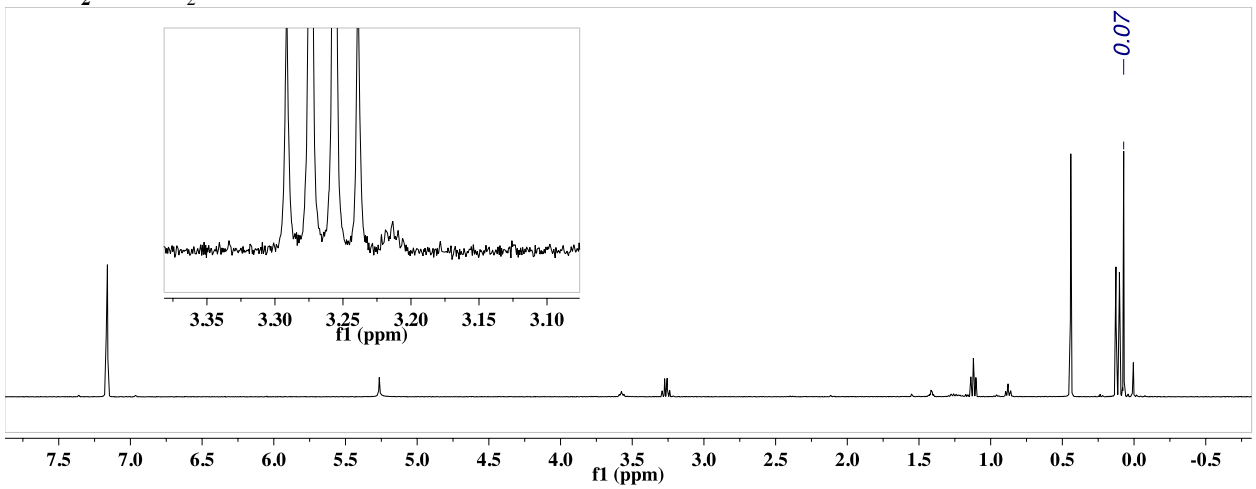

Figure S8.7: ^{1}H NMR (400 MHz) spectrum of the product mixture generated from the reaction of a mixture of **6** and **6-D$_2$** (1:1) with H_2.

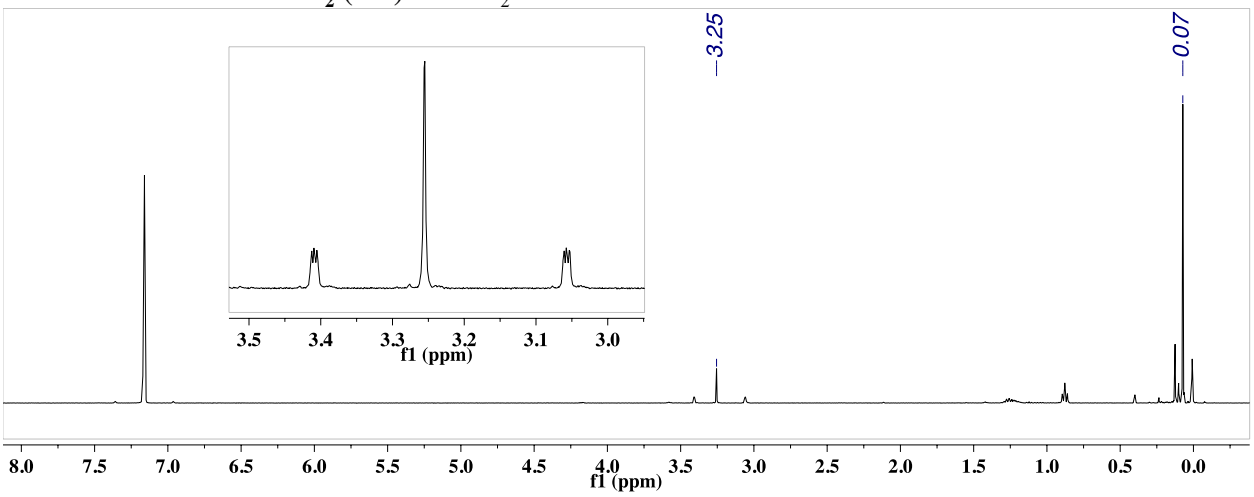

9. Crystallographic Details

	2	**3**	**4**	**5**	**6**
Crystal system	Monoclinic	Monoclinic	Monoclinic	Monoclinic	Triclinic
Crystal size (mm)	0.11 x 0.18 x 0.42	0.20 x 0.21 x 0.27	0.12 x 0.17 x 0.20	0.14 x 0.14 x 0.22	0.13 x 0.21 x 0.27
Formula	$C_{197.8}H_{311.8}B_4Fe_4K_8O_{10}P_{12}$	$C_{41}H_{64}BFeKO_2P_3$	$C_{53}H_{87}BFeKO_5P_3$	$C_{37}H_{55}BFeOP_3$	$C_{41.3}H_{68.3}BFeO_{1.3}P_3Si$
Formula weight (g/mol)	3800.66	787.55	1002.89	675.38	773.74
Space group	P 21/c	P 21/n	P 21/c	P 21/c	P-1
a (Å)	18.8485(17)	14.965(2)	11.2309(19)	10.9781(13)	10.9056(7)
b (Å)	41.389(4)	19.074(3)	23.142(4)	15.8664(18)	11.3906(7)
c (Å)	26.821(3)	16.191(2)	20.143(3)	20.543(2)	20.2061(14)
α (deg)	90	90	90	90	78.666(2)
β (deg)	99.494(4)	103.987(5)	97.191(6)	103.016(4)	78.736(2)
γ (deg)	90	90	90	90	62.016(2)
Z	4	4	4	4	2
V (Å^3)	20638(3)	4484.6(11)	5194.1(15)	3486.3(7)	2157.9(2)
Indep. Reflections	51181	7998	25208	13298	8802
R(int)	0.139	0.072	0.073	0.040	0.130
R1	9.50	9.20	4.58	2.67	7.16
wR2	20.29	30.62	12.08	7.09	18.70
GOF	1.12	1.04	1.02	1.03	1.04

Remarks on Crystal Structures:

Figure S9.1: Crystal structure of **2** showing its crystallization in which four Fe centers and eight K countercations crystallize in a cluster. Hydrogen atoms, five K-coordinated THF molecules, free solvent molecules, and a disordered isopropyl group are omitted.

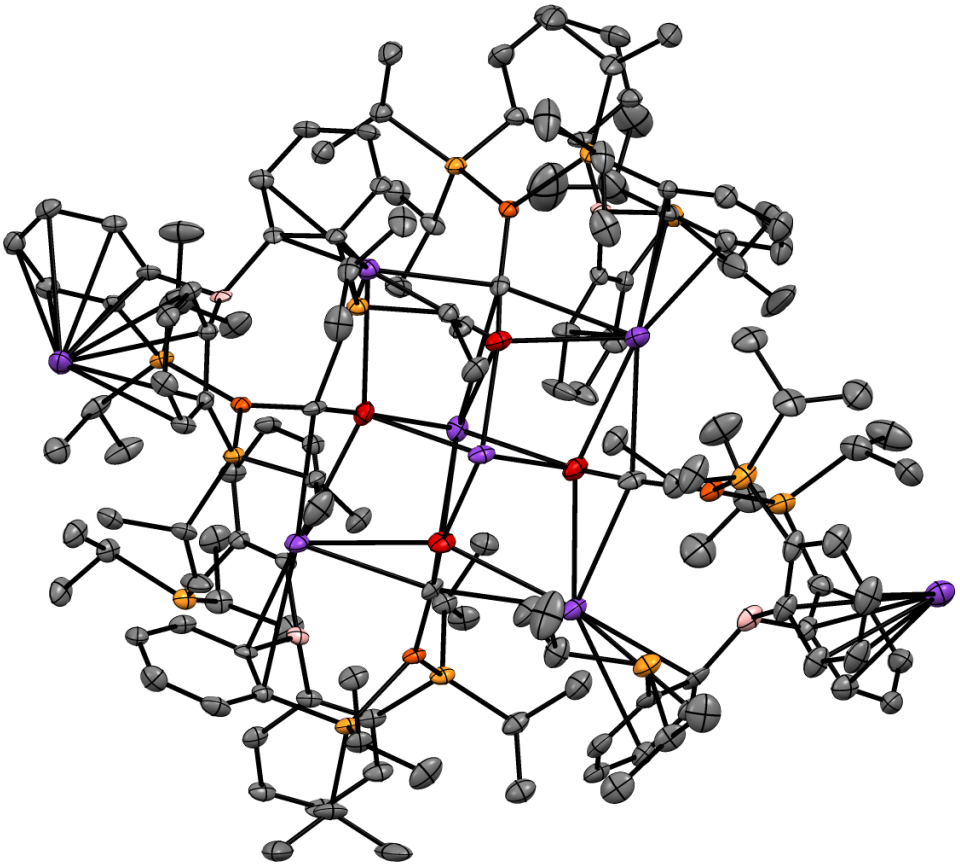

Compound 2. This compound crystallizes as a four Fe, eight K cluster, with four crystallographically independent Fe centers in the asymmetric unit as depicted above. The complex crystallizes with five K-coordinated THF molecules. Some of the hydride ligands could be located in the difference map and refined. For two of the iron centers, the terminal hydride could be refined; for one of the iron centers, the bridging borohydride could be refined; and for the final iron center, both the bridging and terminal borohydride ligands could be refined. One of the ligand isopropyl groups was disordered over two positions (60:40), with refinement aided by the application of a RIGU restraint. Free solvent molecules were found in six positions in the unit cell, including two benzene molecules. A third position was refined as a disordered pentane molecule (77:23). Two positions were refined as mixed THF/pentane disorders (77:23 and 64:36). The final position was refined as a partially occupied (0.7) disorder of benzene and THF (41:29). Refinement of these disorders was aided by the application of RIGU and SIMU restraints and EADP constraints where appropriate.

Compound 3. 3 crystallizes with a K-coordinated THF molecule in the asymmetric unit. This complex cocrystallizes with a minor component of an additional Fe complex that has an intact Fe-B interaction (likely **4** based on NMR obtained of crystalline material) (90:10). Only the

heavy atoms of this minor component (Fe and 3 P) could be refined with the aid of a RIGU restraint. The phenylene rings associated with the Fe-coordinated phosphines are also disordered over two positions (62:38 and 71:29). RIGU restraints and an AFIX 66 command aided with refinement of this disorder. The coordinated THF molecule was refined as disordered over two positions (65:35). Refinement of this disorder was aided by the application of RIGU and SADI restraints. The borohydride ligand and one of the hydride ligands could be located and refined freely.

Compound 4. 4 crystallizes with two K-coordinated THF molecules and two free THF molecules in the asymmetric unit. The bridging borohydride and one of the terminal iron hydrides could be refined. The two coordinated THF molecules were modeled as disordered over two positions (70:30 for both). Disorder refinement of K-coordinated THF molecules was aided by a RIGU restraint. One of the free THF molecules was refined as disordered over two positions (72:28). The second THF was refined as disordered over three positions (50:38:12). Anisotropic refinement of free THF molecules was aided by the application of RIGU, SADI, and SAME restraints.

Compound 5. 5 crystallizes in the absence of solvent.

Compound 6. 6 crystallizes with a partially occupied Et_2O molecule, which is disordered over a special position. Each of the three phosphine ligands has an independently disordered isopropyl group. Two of the isopropyl groups are disordered over two positions (56:44 and 74:26) while the third is disordered over three positions (37:36:27). Refinement of these disorder components was aided by the application of RIGU restraints. The axial CH_2OSiMe_3 ligand is disordered over two positions (64:36) and refinement of this disorder is aided by the application of a RIGU restraint and an EADP constraint.

10. Bond Distances and Angles

Compound 2.

Bond Distances (Å)		Bond Angles (degrees)	
Fe1			
Fe1-P1 (coord.)	2.171(2)	P1-Fe1-P2	116.32(6)
Fe1-P2 (coord.)	2.206(2)	Fe1-C0AA-O1	174.7(5)
Fe1-P3 (free)	6.183(2)	B1-Fe1-C0AA	110.7(2)
Average Fe-P (coord.)	2.19	P1-Fe1-C0AA	115.0(2)
Fe1-C0AA	1.698(6)	P2-Fe1-C0AA	128.5(2)
Fe1-B1	2.783(5)		
Fe1-H1-B1	1.59(5)		
Fe1-H	1.48(5)		
C0AA-O1	1.235(7)		
Fe2			
Fe2-P4 (coord.)	2.180(2)	P4-Fe2-P5	126.52(6)
Fe2-P5 (coord.)	2.152(1)	Fe2-C38-O2	174.5(5)
Fe2-P6 (free)	4.603(2)	B2-Fe2-C38	116.5(2)
Average Fe-P (coord.)	2.17	P4-Fe2-C38	118.1(2)
Fe2-C38	1.709(5)	P5-Fe2-C38	115.0(2)
Fe2-B2	2.764(6)		
Fe2-HB	1.49(8)		
C38-O2	1.225(6)		
Fe3			
Fe3-P7 (coord.)	2.212(2)	P7-Fe3-P8	117.60(6)
Fe3-P8 (coord.)	2.187(1)	Fe3-C75-O3	175.1(5)
Fe3-P9 (free)	6.189(2)	B3-Fe3-C75	109.8(2)
Average Fe-P (coord.)	2.20	P7-Fe3-C75	127.8(2)
Fe3-C75	1.693(5)	P8-Fe3-C75	114.2(2)
Fe3-B3	2.785(6)		
Fe3-H3A-B3	1.59(6)		
C75-O3	1.239(6)		
Fe4			
Fe4-P10 (coord.)	2.172(2)	P10-Fe4-P11	121.86(7)
Fe4-P11 (coord.)	2.160(2)	Fe4-C111-O4	175.0(5)
Fe4-P12 (free)	4.894(2)	B4-Fe4-C111	116.0(2)
Average Fe-P (coord.)	2.17	P10-Fe4-C111	121.2(2)
Fe4-C111	1.704(5)	P11-Fe4-C111	116.3(2)
Fe4-B4	2.763(6)		
Fe4-HA	1.61(6)		
C111-O4	1.246(6)		
Average Over Asymmetric Unit			
Fe-P (coord.)	2.18 ± 0.02	P-Fe-P	120.6 ± 4.6
Fe-C	1.70 ± 0.01	Fe-C-O	174.8 ± 0.3
Fe-B	2.77 ± 0.01	B-Fe-C	113.3 ± 3.5

C-O	1.24 ± 0.01	P-Fe-C	119.5 ± 5.7

Compound 3.

Bond Distances (Å)		Bond Angles (degrees)	
Fe1-P1 (coord.)	2.171(3)	P1-Fe1-P2	153.2(1)
Fe1-P2 (coord.)	2.143(2)	P1-Fe1-C1	106.8(2)
Fe1-P3 (free)	4.400(3)	P2-Fe1-C1	100.0(2)
Average Fe-P (coord.)	2.16	Fe1-C1-O1	171.4(6)
Fe1-C1	1.743(7)	B1-Fe1-C1	116.6(3)
Fe1-B1	2.687(6)		
Fe1-H1A-B1	1.802		
Fe1-H	1.54(7)		
C1-O1	1.184(8)		

Compound 4.

Bond Distances (Å)		Bond Angles (degrees)	
Fe1-P1	2.2166(7)	P1-Fe1-P2	105.57(2)
Fe1-P2	2.1695(6)	P2-Fe1-P3	137.73(2)
Fe1-P3	2.2167(6)	P1-Fe1-P3	109.64(2)
Average Fe-P	2.20	Fe1-C0-O1	177.7(1)
Fe1-C0	1.741(1)	B1-Fe1-C0	178.51(6)
Fe1-B1	2.332(1)	P1-Fe1-C0	102.04(4)
Fe1-H	1.46(3)	P2-Fe1-C0	96.14(4)
C0-O1	1.189(2)	P3-Fe1-C0	98.62(4)

Compound 5.

Bond Distances (Å)		Bond Angles (degrees)	
Fe1-P1	2.2954(5)	P1-Fe1-P2	115.86(2)
Fe1-P2	2.3444(4)	P2-Fe1-P3	132.81(2)
Fe1-P3	2.2536(4)	P1-Fe1-P3	101.73(2)
Average Fe-P	2.30	Fe1-C1-O1	178.95(9)
Fe1-C1	1.746(1)	B1-Fe1-C1	178.64(4)
Fe1-B1	2.650(1)	P1-Fe1-C1	100.60(4)
Fe1-H1-B	1.53(1)	P2-Fe1-C1	100.47(4)
C1-O1	1.158(1)	P3-Fe1-C1	99.45(4)

Compound 6.

Bond Distances (Å)		Bond Angles (degrees)	
Fe1-P1	2.425(2)	P1-Fe1-P2	113.63(5)
Fe1-P2	2.395(1)	P2-Fe1-P3	107.59(5)
Fe1-P3	2.348(1)	P1-Fe1-P3	119.09(5)
Average Fe-P	2.39	Fe1-C1A-O1A	113.5(7)
Fe1-C1A	2.07(1)	Fe1-C1B-O1B	104(1)
Fe1-C1B	2.08(2)	B1-Fe1-C1A	173.1(3)
Fe1-B1	2.489(4)	B1-Fe1-C1B	90.7(5)
C1A-O1A	1.46(1)	P1-Fe1-C1A	99.3(3)
C1B-O1B	1.42(2)	P2-Fe1-C1A	108.9(3)
		P3-Fe1-C1A	107.6(3)
		P1-Fe1-C1B	115.1(5)
		P2-Fe1-C1B	108.3(5)
		P3-Fe1-C1B	90.7(5)

11. Reaction of 2 with Stoichiometric R_3SiOTf

A solution of **2** (in THF, THF-d_8 or 2-MeTHF) was generated *in situ* and cooled to -78 °C. $^{i}Pr_3SiOTf$ (1 equiv) was added as a dilute solution in Et_2O. The mixture was stirred at -78 °C for 15 min then at room temperature for 15 min slowly turning dark red-orange. A mixture of species is generated, with a single diamagnetic species as the major product as judged by NMR spectroscopy. We have tentatively assigned this species as the monoanionic product of CO-functionalization in which the silyl electrophile has reacted at the carbonyl O, one hydride equivalent has migrated to the carbonyl C, with the stabilization of this species by a P-C interaction. This motif is related to the phosphine-trapped η^2-formyl complex reported by Fryzuk and coworkers.[3] Reaction impurities and decomposition of the product precluded isolation and crystallization of this species. Similar products were observed with related silyl electrophiles (Me_3SiOTf, $^{t}BuMe_2SiOTf$) but reactions using $^{i}Pr_3SiOTf$ generally proceeded most cleanly. Once this species is formed, it does not generate **6** upon the addition of stoichiometric oxidant or an additional electrophile equivalent. We hypothesize that this is due to irreversible P-C bond formation, preventing the formation of **6**. If this is the case, in the presence of excess R_3SiOTf, productive formation of **6** requires oxidation to proceed more quickly than P-C bond formation.

$^{31}P\{^{1}H\}$ NMR (THF-d_8; 162 MHz): δ 79.1 (dd, J = 140, 13 Hz), 74.3 (dd, J = 140, 9 Hz), 55.6 (dd, J = 13, 9 Hz). $^{31}P\{^{1}H\}$ NMR (THF-d_8; ^{13}CO-labeled; 162 MHz): δ 79.1 (dd, J = 140, 13 Hz), 74.3 (dd, J = 140, 9 Hz), 55.6 (ddd, J = 66, 13, 9 Hz). $^{13}C\{^{1}H\}$ NMR (2-MeTHF; ^{13}CO-labeled; 101 MHz): δ 24.1 (br). ^{1}H NMR (THF-d_8; 400 MHz): δ 8.42 (d, J = 7.7 Hz, 1H), 8.28 (d, J = 7.7 Hz, 1H), 8.17 (d, J = 7.4 Hz, 1H), 7.27 (overlapping m, 2H), 7.19 (t, J = 7.5 Hz, 1H), 7.06 (t, J = 7.4 Hz, 1H), 7.00 (t, J = 7.3 Hz, 1H), 6.85 (overlapping m, 2H), 6.77 (t, J = 7.4 Hz, 1H), 6.57 (br m, 1H), 2.7-1.9 (^{i}Pr C-*H*, 7 H), 1.2-0.5 (^{i}Pr CH_3, 42H), -0.55 (dt, J = 13, 9 Hz, 1H), -9.85 (br, Fe-*H*, 1H). ^{1}H NMR (THF-d_8; ^{13}C-labeled; 400 MHz): δ 8.42 (d, J = 7.7 Hz, P-C-*H*, 1H), 8.28 (d, J = 7.7 Hz, 1H), 8.17 (d, J = 7.4 Hz, 1H), 7.27 (overlapping m, 2H), 7.19 (t, J = 7.5 Hz, 1H), 7.06 (t, J = 7.4 Hz, 1H), 7.00 (t, J = 7.3 Hz, 1H), 6.85 (overlapping m, 2H), 6.77 (t, J = 7.4 Hz, 1H),

(3) Fryzuk, M. D.; Mylvaganam, M.; Zaworotko, M. J.; MacGillivray, L. R. *Organometallics* **1996**, *15*, 1134.

6.57 (br m, 1H), 2.7-1.9 (^{i}Pr C-*H*, 7 H), 1.2-0.5 (^{i}Pr CH_3, 42H), -0.55 (ddt, *J* = 127, 13, 9 Hz, 1H), -9.85 (br, Fe-*H*, 1H).

Figure S11.1: Proposed structure of the diamagnetic product generated upon the reaction of **2** with stoichiometric ^{i}Pr$_3$SiOTf.

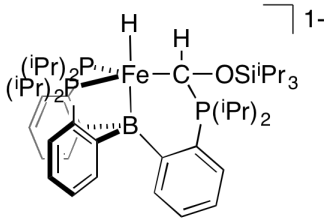

Figure S11.2: ^{1}H NMR (THF-d_8; 400 MHz) spectrum from the reaction of **2** with stoichiometric ^{i}Pr$_3$SiOTf. Note: ^{i}Pr resonances are poorly resolved and overlapping with paramagnetic impurities and added Et_2O.

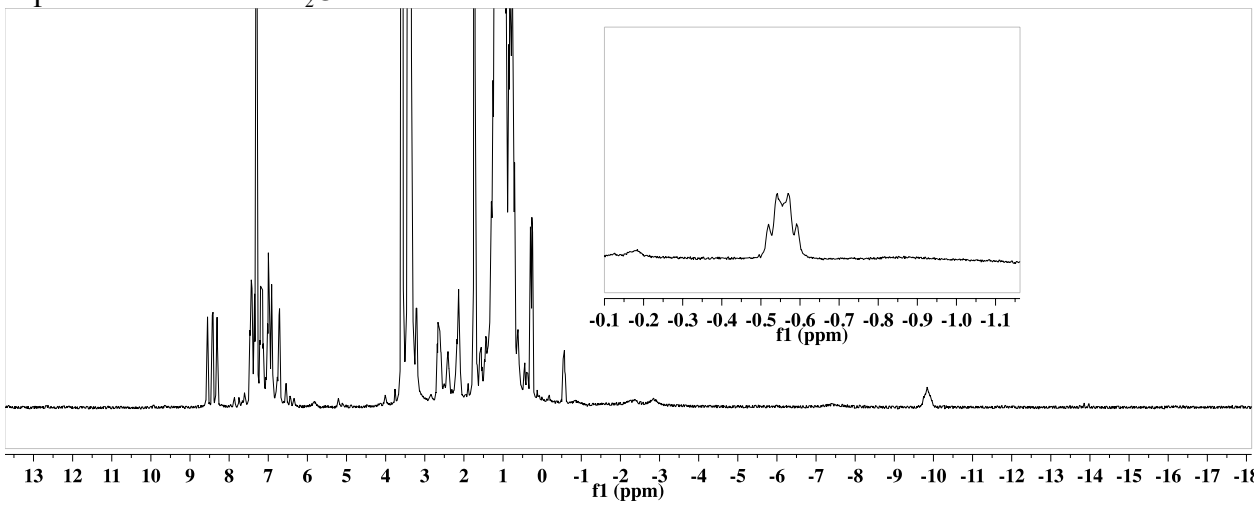

Figure S11.3: ^{1}H NMR (THF-d_8; 400 MHz) spectrum from the reaction of **2**-^{13}**CO** with stoichiometric ^{i}Pr$_3$SiOTf.

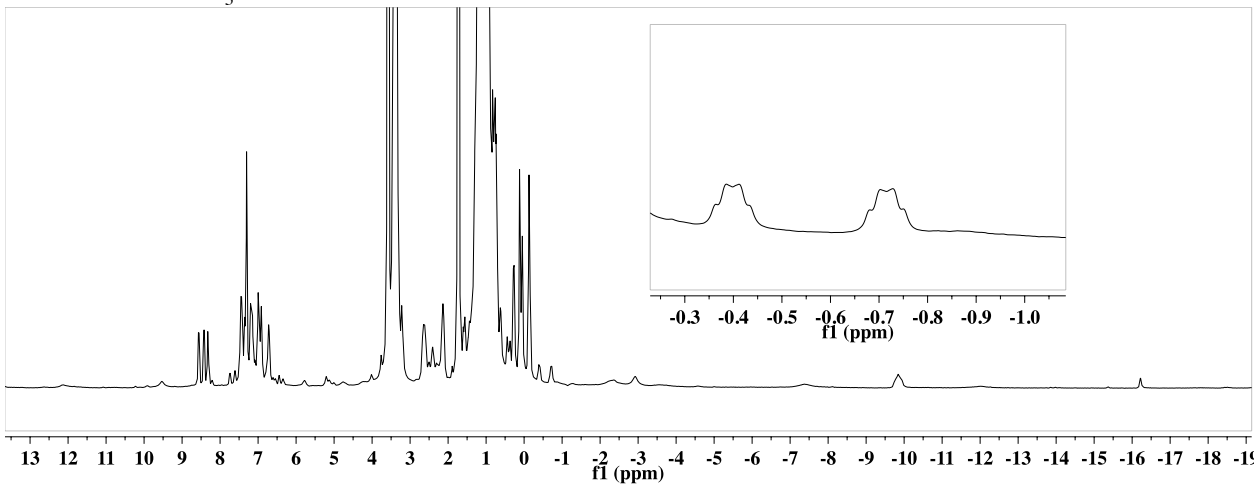

Figure S11.4: ^{1}H NMR (THF-d_8; 400 MHz) spectrum from the reaction of **2**-$\mathbf{D_2}$ with stoichiometric $^{i}Pr_3SiOTf$. Note the observation of the hydridic resonance at -9.85 ppm is consistent with scrambling of the ligand into this position, which is observed for hydride species supported by this scaffold that can access lower coordinate states. For example, P_3^B(μ-H)Fe(H)(L) undergoes scrambling when L is labile (L = H_2, N_2), but not in the case of stronger axial donors (L = CO).[4]

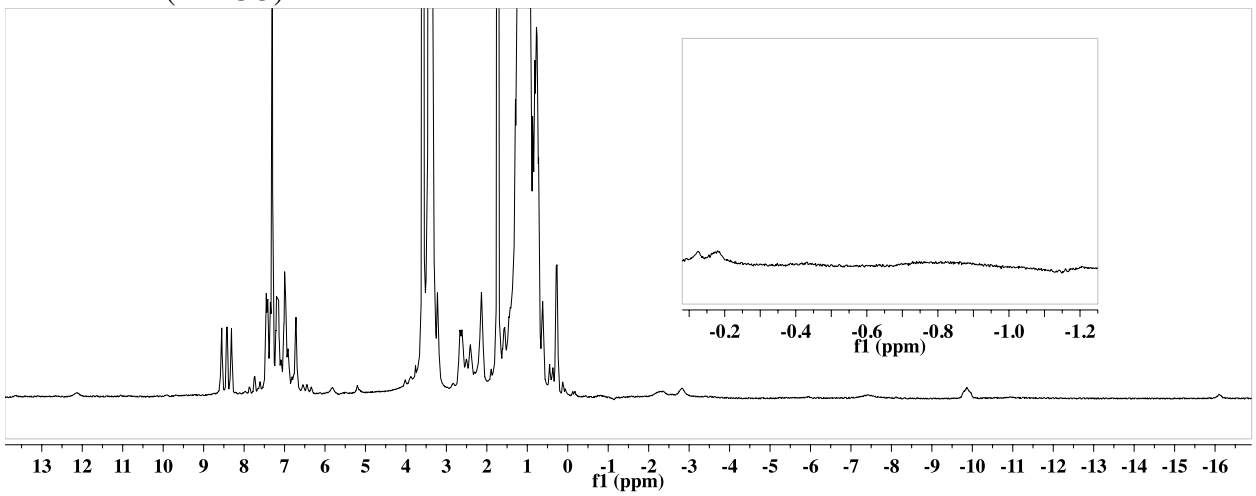

Figure S11.5: $^{31}P\{^{1}H\}$ NMR (THF-d_8; 162 MHz) spectrum from the reaction of **2** with stoichiometric $^{i}Pr_3SiOTf$.

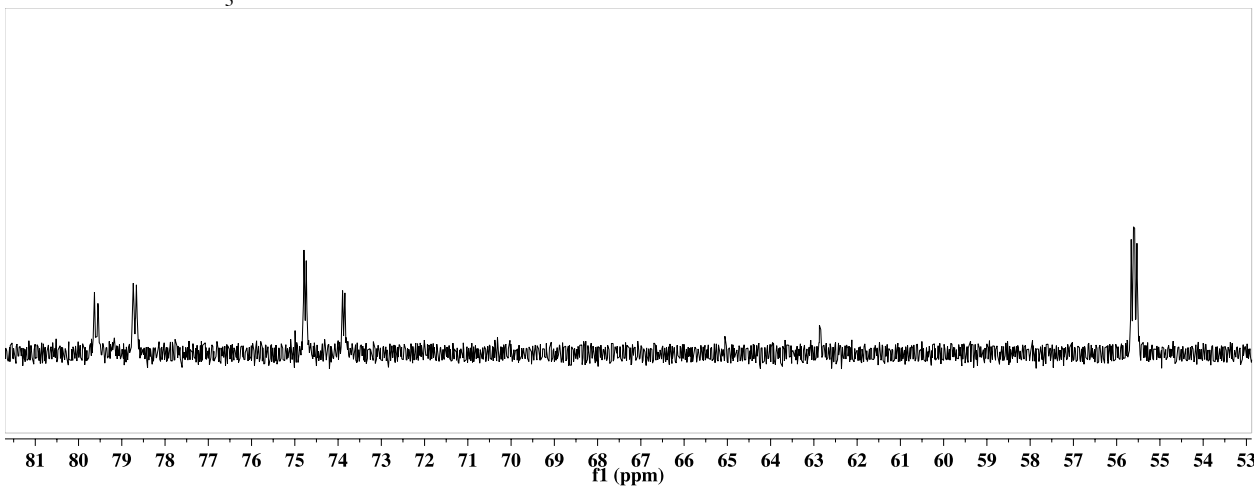

(4) Fong, H.; Moret, M.-E.; Peters, J. C. *Organometallics* **2013**, *32*, 3053.

Figure S11.6: $^{31}P\{^{1}H\}$ NMR (THF-d_8; 162 MHz) spectrum from the reaction of **2-^{13}CO** with stoichiometric $^{i}Pr_3SiOTf$.

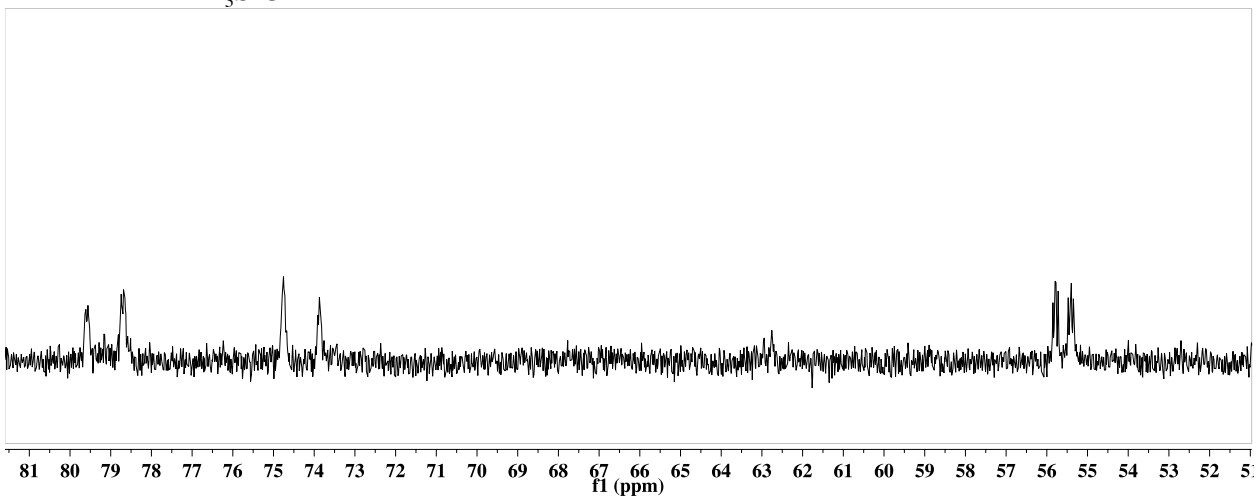

Figure S11.7: ^{13}C NMR (2-MeTHF; 101 MHz) spectrum from the reaction of **2-^{13}CO** with stoichiometric $^{i}Pr_3SiOTf$. Solvent resonances observable are consistent with 2-MeTHF, added C_6D_6, and Et_2O used in the electrophile dilution. In THF, the product resonance directly overlapped with the solvent resonance.

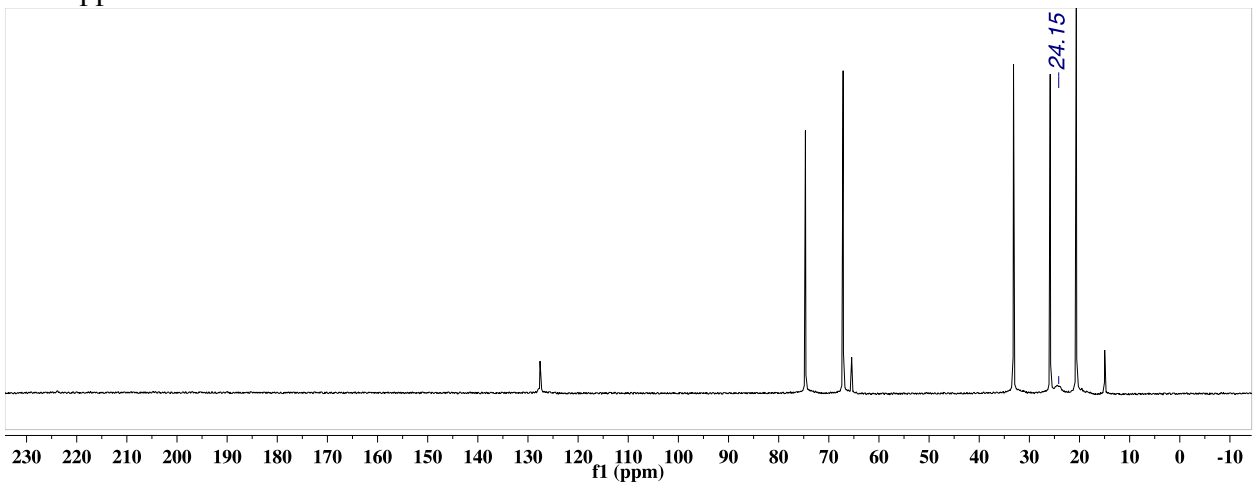

Figure S11.8: ^{13}C-HSQC (THF-d_8) spectrum from the reaction of **2-^{13}CO** with stoichiometric $^{i}Pr_3SiOTf$.

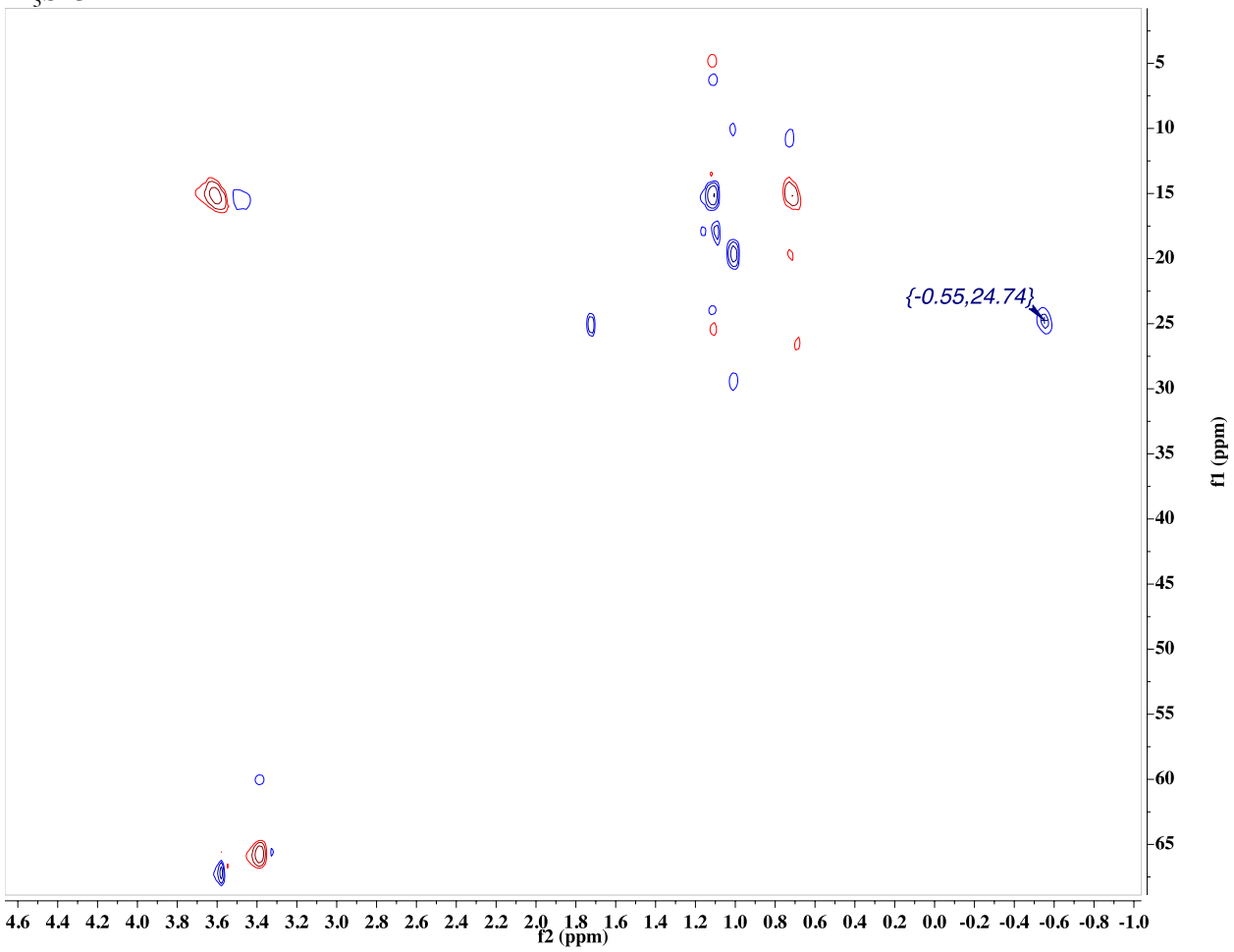

12. Reaction of 6 with H_2 and $PhSiH_3$ with PMe_3 Added

Following the reaction of **6** with H_2 or $PhSiH_3$, the terminal Fe-containing mixture is intractable in the absence of additives and dependent on the choice of E-H source (H_2 or $PhSiH_3$). To remedy this problem, we explored the addition of coordinating ligands in these reaction mixtures. We found that CO and ^{t}BuNC reacted quickly with **6**, and no product release was observed in the presence of these additives. When these reactions were carried out with added PMe_3 (5 equiv), similar yields of the free organic products (E-CH_2OSiMe_3) were obtained (H_2: 59%; $PhSiH_3$: 42%; single experiments). Further, the same mixture of Fe-containing products is observed by NMR spectroscopy, with new, paramagnetically shifted resonances (peak picked here) along with an observable amount of **1**. This is consistent with the Mössbauer data, which shows a mixture of **1**, a new S = 3/2 species, and a residual signal that is likely representative of multiple species (see below).

Figure S12.1: ^{1}H NMR (C_6D_6; 400 MHz) spectrum of the reaction of **6** with H_2 (1 atm) with an excess of PMe_3 added (5 equiv). Peaks corresponding to a residual amount of **6** are observable.

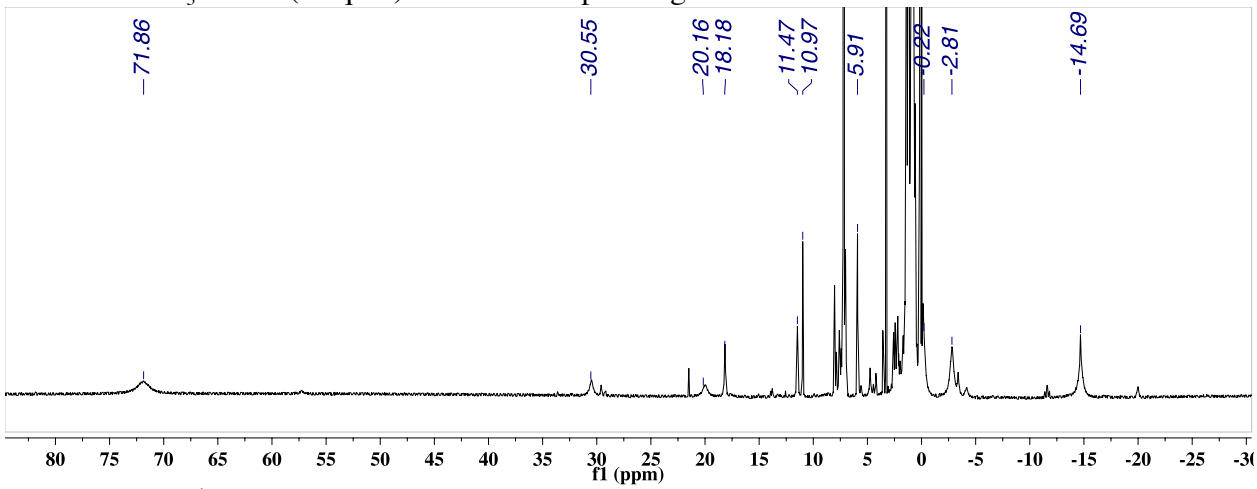

Figure S12.2: ^{1}H NMR (C_6D_6; 400 MHz) spectrum of the reaction of **6** with $PhSiH_3$ (5 equiv) with an excess of PMe_3 added (5 equiv). Peaks corresponding to diamagnetic **1** are also observed.

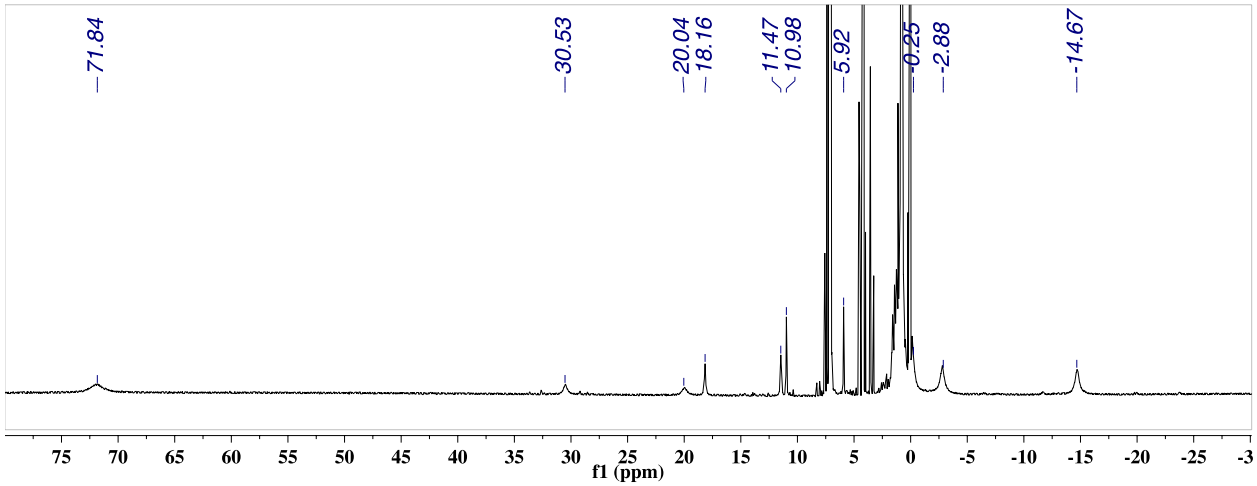

Figure S12.3: Mössbauer spectrum (77 K; benzene; 50 mT) of the reaction of **6** with $PhSiH_3$ (5 equiv) with an excess of PMe_3 added (5 equiv). The spectrum could be fit as a mixture of three components. In blue, the largest component (δ = 0.52; ΔE_Q = 0.69; 41%) has parameters consistent with an S = 3/2 complex supported by this scaffold. The species in green (δ = 0.02; ΔE_Q = 1.08; 35%) has parameters consistent with **1** and is observable in the ^{1}H NMR spectrum. The third species in orange (δ = 0.69; ΔE_Q = 1.55; 24%) has an isomer shift consistent with intermediate-to-high spin iron for this system (S = 3/2 or S = 2), but is quite broad and is likely representative of multiple species.[5]

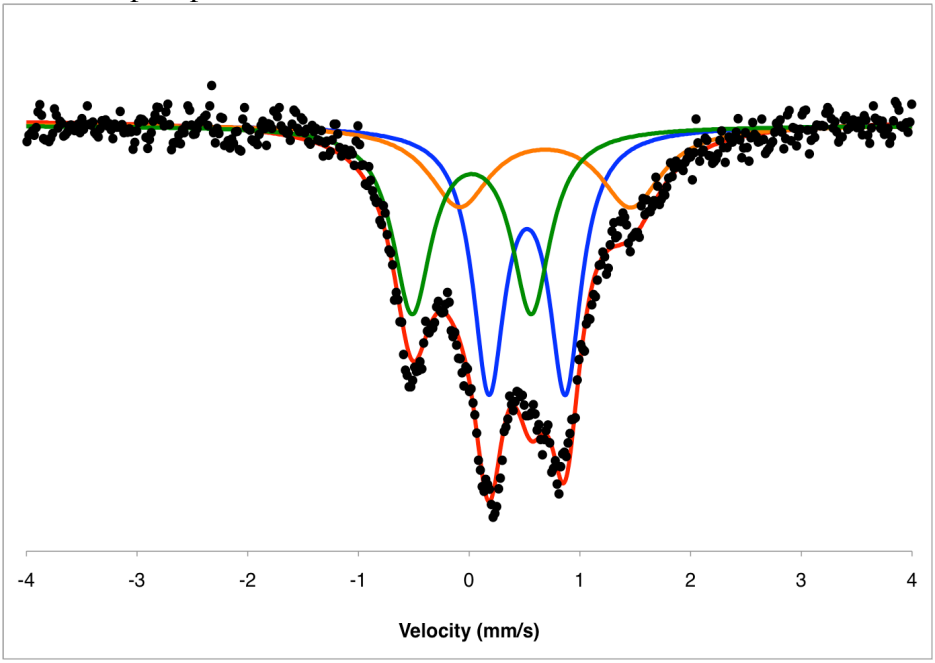

(5) A discussion of the correlation between isomer shift and spin state for P_3^BFe-containing compounds can be found in: Del Castillo, T. J.; Thompson, N. B.; Peters, J. C. *J. Am. Chem. Soc.* **2016**, *138*, 5341.